HHS Public Access

Author manuscript

Nat Protoc. Author manuscript; available in PMC 2019 October 01.

Published in final edited form as:

Nat Protoc. 2018 October ; 13(10): 2362–2386. doi:10.1038/s41596-018-0042-5.

Analysis of redox landscapes and dynamics in living cells and *in vivo* using genetically encoded fluorescent sensors

Yejun Zou[1,3,7], **Aoxue Wang**[1,3,7], **Mei Shi**[1,3], **Xianjun Chen**[1,3], **Renmei Liu**[1,3], **Ting Li**[1,3], **Chenxia Zhang**[1,3], **Zhuo Zhang**[1,3], **Linyong Zhu**[4], **Zhenyu Ju**[5], **Joseph Loscalzo**[6], **Yi Yang**[1,2], **Yuzheng Zhao**[1,3]

[1]Synthetic Biology and Biotechnology Laboratory, State Key Laboratory of Bioreactor Engineering, Shanghai Collaborative Innovation Center for Biomanufacturing Technology, East China University of Science and Technology, 130 Mei Long Road, Shanghai 200237, China

[2]Optogenetics & Synthetic Biology Interdisciplinary Research Center, CAS Center for Excellence in Brain Science, Shanghai Institutes for Biological Sciences, Chinese Academy of Sciences, Shanghai 200031, China

[3]Shanghai Key Laboratory of New Drug Design, School of Pharmacy, East China University of Science and Technology, 130 Mei Long Road, Shanghai 200237, China

[4]School of Chemistry and Molecular Engineering, East China University of Science and Technology, Shanghai, China.

[5]Key Laboratory of Regenerative Medicine of Ministry of Education, Institute of Aging and Regenerative Medicine, Jinan University, Guangzhou 510632, China.

[6]Department of Medicine, Brigham and Women's Hospital, Harvard Medical School, Boston, Massachusetts, USA.

[7]These authors contributed equally to this work.

Abstract

Cellular oxidation-reduction reactions are mainly regulated by pyridine nucleotides (NADPH/$NADP^+$ and NADH/NAD^+), thiols and reactive oxygen species (ROS), and play central roles in cell metabolism, cellular signaling and cell fate decisions. A comprehensive evaluation or

Correspondence should be addressed to Y. Zhao (yuzhengzhao@ecust.edu.cn) and Y.Y. yiyang@ecust.edu.cn).

AUTHOR CONTRIBUTIONS

Y. Zhao, Y.Y., Y. Zou and M.S. conceived and designed the live cell and zebrafish imaging experiments. Y. Zhao, Y.Y. and A.W. designed the flow cytometry analysis experiment. Y. Zou, A.W., M.S., X.C., R.L., T.L., C.Z. performed experiments. Z.Z., L.Z., Z.J., and J.L. gave technical support and conceptual advice. Y.Y., Y. Zhao, Y. Zou, A.W., M.S., and J.L. analyzed the data and wrote the manuscript.

Up to four primary research articles where the protocol has been used and/or developed:

1. Tao R, Zhao Y, Chu H, et al. Genetically encoded fluorescent sensors reveal dynamic regulation of NADPH metabolism. *Nature Methods*, 2017,14(7):720–728

2. Zhao Y, Hu Q, Cheng F, et al. SoNar, a highly responsive NAD^+/NADH sensor, allows high-throughput metabolic screening of anti-tumor agents. *Cell Metabolism*, 2015, 21(5): 777–789

3. Zhao Y, Wang A, Zou Y, et al. In vivo monitoring of cellular energy metabolism using SoNar, a highly responsive sensor for NAD(+)/NADH redox state. *Nature Protocols*, 2016, 11(8): 1345–1359

COMPETING FINANCIAL INTERESTS

The authors declare no competing financial interests.

multiplex analysis of redox landscapes and dynamics in intact living cells is important for interrogating cell functions in both healthy and diseased states; however, until recently, this goal has been limited owing to the lack of a complete set of redox sensors. We recently reported a series of highly responsive, genetically encoded fluorescent sensors for NADPH, significantly strengthening the existing toolset of genetically encoded sensors for thiols, H_2O_2, and NADH redox states. By combining sensors with unique spectral properties and specific sub-cellular targeting domains, our approach allows for simultaneous imaging of up to four different sensors. In this protocol, we first describe strategies for multiplex fluorescence imaging of these sensors in single cells, and we demonstrate how to apply these sensors to study changes in redox landscapes during the cell cycle, following macrophage activation, and in living zebrafish. This approach can be adapted to different genetically encoded fluorescent sensors using various analytical platforms, such as fluorescence microscopy, high-content imaging systems, flow cytometry, and microplate readers. Typically, the preparation of cells or zebrafish expressing different sensors is anticipated to take 2–3 d, and microscopy imaging or flow cytometry analysis can be performed in 5–60 min.

Keywords

NADPH; NADH; thiol redox; H_2O_2; genetically encoded fluorescent sensors; real-time imaging; live cell imaging; *in vivo* imaging

INTRODUCTION

Oxidation-reduction reactions play central roles in cell metabolism and are integral components of cellular signaling and cell fate decisions. Cellular redox states are mainly governed by pyridine nucleotides (NADPH/$NADP^+$ and NADH/NAD^+), thiols, and reactive oxygen species (ROS), which form a complex network of interactions (Fig. 1). Among them, both NADPH and NADH are from glucose catabolism in the cytosol and the citrate acid cycle in the mitochondria; however, they engage in distinct metabolic pathways[1]. NADPH governs fatty acid, nucleotide and amino acid biosynthetic pathways[2] and provides reducing power for thiol redox networks, such as glutathione (GSH) systems and thioredoxin (Trx) systems, which then scavenge ROS and repair ROS-induced damage[3,4]. In addition, NADPH can also be used to generate ROS through the tightly regulated NADPH oxidase activity in addition to NADH-dependent ROS generation in mitochondria[4,5] (Fig. 1). In contrast, NADPH's dephosphorylated form, NADH, plays a central role in cellular energy metabolism and drives ATP production in the cytosol by glycolysis and in the mitochondria by oxidative phosphorylation[6] (Fig. 1).

NADPH is generally thought to be generated primarily via the oxidative pentose phosphate pathway (PPP)[7]. However, other potential sources of NADPH exist in mammalian cells, including reactions catalyzed by isocitrate dehydrogenase (IDH1/2), malic enzyme (ME1/3), methylene tetrahydrofolate dehydrogenase (MTHFD1/2), glutamate dehydrogenase (GDH), aldehyde dehydrogenase (ALDH), and nicotinamide nucleotide transhydrogenase (NNT)[2,7,8]. Among them, MTHFD-mediated serine/glycine metabolism is a significant source of NADPH[2,7]. NADH in the cytosol is generated primarily by glycolytic reactions and is then consumed during the reduction of pyruvate into lactate[1]. NADH in the

mitochondria mainly produces from pyruvate decarboxylation and the citrate acid cycle[1]. NADH and NADPH are connected by mitochondrial NNT[1].

The redox states of pyridine nucleotides, thiols, and ROS are highly compartmentalized and dynamic; maintaining redox homeostasis is vital for the execution of compartment-specific redox processes. Perturbation of redox metabolism leads to impaired cellular functions, thereby increasing the risks of numerous disease-associated pathologies[4,5]. Therefore, a comprehensive evaluation or multiplex analysis of redox landscapes and dynamics in living cells is crucial for interrogating cell functions in both healthy and diseased states.

Methods for redox analysis

Traditional biochemical methods for the analysis of redox states of specific metabolites, i.e., chromatography, mass spectrometry, enzymatic cycling assays[9,10], capillary electrophoresis[11], and isotope-labeling techniques[2,12], are invasive and do not capture the transient subcellular redox changes associated with metabolic activation or dysfunction in intact individual cells. Furthermore, these methods all suffer from potential sample oxidization or degradation during processing, potentially leading to spurious measurements of the redox-active species. Alternatively, researchers have used the autofluorescence of some redox metabolites (i.e., NADPH, NADH, and Flavin adenine dinucleotide (FAD) to monitor the cellular redox state[6,13]. Unfortunately, NADPH and NADH have similar spectral properties and are difficult to differentiate optically, although they have distinct functions in cells.

To monitor the cellular redox state and dynamics spatiotemporally, genetically encoded fluorescent sensors were developed, targeted to subcellular organelles, and used to monitor redox states of living cells (Table 1). Very recently, we reported a series of highly responsive, genetically encoded fluorescent sensors for NADPH[8], which significantly strengthen the existing toolset of genetically encoded sensors for thiols[14–17], H_2O_2[18–21] and NADH[22–24] redox states. Together, these sensors should advance the study of redox biology[25].

Genetically encoded NADPH sensors

Genetically encoded fluorescent sensors have become potent optical tools for monitoring cellular states and events[26]. A few genetically encoded NADH sensors have recently been developed by coupling fluorescent proteins to the NADH binding domain of the bacterial repressor Rex, permitting the monitoring of dynamic changes in NADH levels and cellular energy metabolism states[22,24,27,28]. We have recently developed SoNar, a highly responsive NADH/NAD^+ sensor that has superior properties, including intense fluorescence, rapid responsiveness, pH insensitivity, and a wide dynamic range, enabling the sensor to be useful not only for microscopy but also for *in vivo* imaging[22,23,29]. As the molecular structure of NADPH is very similar to that of NADH, with only one additional phosphate group at the 2’-position of the ribose ring, we reasoned that SoNar could be used as a template for designing an NADPH sensor. Following structural bioinformatics analysis of ligand selectivity in natural NAD(H)-binding and NADP(H)-binding proteins, we successfully engineered NADPH sensors by introducing mutations into SoNar that switch the charges

and hydrophobicity, and eliminate the steric hindrance of ligand binding. As a result, a series of NADPH sensors, iNap1 to iNap4, were obtained and characterized[8]. iNap sensors are intrinsically ratiometric with two excitation wavelengths and have opposing responses to NADPH-binding when excited at 420 nm and 485 nm, leading to 500%−1000% ratiometric fluorescence changes (Fig. 2a, b). Fluorescence titration studies showed that iNap 1–4 sensors have apparent dissociation constants (K_d) of ~2.0 μM, ~6.0 μM, ~25 μM, and ~120 μM, respectively (Fig. 2c). Thus, iNap sensors with various affinities further expand their applications in different cells and subcellular organelles. For mammalian cells, we suggest iNap1/2 for measurement of low-abundance cytosolic NADPH and iNap3 for measurement of higher-concentration mitochondrial NADPH[8]. Unlike the NADH/NAD^+ ratio sensor SoNar, the iNap sensors are only responsive to NADPH concentrations and not to the NADPH/$NADP^+$ ratio. The response of iNap sensors to various NADPH concentrations is not substantially affected by physiological concentrations of free $NADP^+$, suggesting that $NADP^+$ does not compete with NADPH binding to iNap[8]. Therefore, iNap can be used only as an authentic reporter for NADPH. Similar to SoNar, iNap sensors also have favorable characteristics, such as intense fluorescence, rapid responsiveness, pH insensitivity, a large dynamic range, targeting to subcellular organelles, and ratiometric imaging and dynamic measurements in living cells and *in vivo*.

Based on the enzymatic reaction equilibrium catalyzed by malic enzyme, isocitrate dehydrogenase, and shikimate dehydrogenase, three different research groups estimate the cytosolic free NADPH/$NADP^+$ ratio to be 15–333[9,30,31] (Table 2), which is much higher than the whole-cell NADPH/$NADP^+$ ratio (typically, 1–3)[9,30,31]. Such a difference may be due to a large fraction of cytosolic $NADP^+$ being bound to protein[30]. To our knowledge, subcellular free NADPH levels in living cells had not been rigorously quantified owing to lack of appropriate quantitative non-invasive methodology. Utilizing iNap sensors, we found that the cytosolic free NADPH level (~3.1 μM) in mammalian cells was one order of magnitude higher than the free NADH level (~0.12 μM), which is slightly greater than the previous estimate of a NADPH/NADH ratio of ~4 (ref.[32]). By contrast, the mitochondrial free NADPH concentration (~37 μM) was estimated to be roughly equal to the free NADH concentration (~30 μM) that we previously measured using the Frex sensor[24] (Table 2), consistent with recent FLIM imaging showing that the enzyme-bound NADPH/NADH ratio is ~0.7 (ref.[6]). Thus, the mitochondrial NADPH pool merits more attention, especially in the endogenous NAD(P)H fluorescence assay, as it makes a comparable contribution to mitochondrial NAD(P)H signals, now widely used for the evaluation of mitochondrial function from animal models to human studies[33]. The relatively high NADPH levels in mitochondria may be essential for scavenging excessive ROS from the electron transport chain, which can disrupt cellular functions through the oxidation of lipids, proteins, and DNA[34].

$NADP^+$, the oxidized form of NADPH, is generated *de novo* from NAD^+ by NADK[5]. Human cells have two compartment-specific NADKs, cytosolic NADK and mitochondrial NADK2[35,36]. Notably, iNap imaging indicated that not only the cytosolic NADPH pool but also the mitochondrial NADPH pool is regulated by cytosol-localized NADK, suggesting that $NADP^+$ produced in the cytoplasm can influence mitochondrial stores. Interestingly, a recent study also suggested that there are multiple sources of mitochondrial NAD^+ and that

cytosolic NAD^+ may be transported into mitochondria[37]. There is currently no direct evidence for the physiological transport of NADP(H) across the inner mitochondrial membrane.

For mammalian cells, we found that measurement of the low abundance of cytosolic NADPH could be performed using iNap1, iNap2, or iNap3 sensors and that measurement of higher mitochondrial NADPH abundances could be performed using iNap2 or iNap3 sensors, with reasonably similar quantitative results. Utilizing iNap sensors, we found that mammalian cells have a strong tendency toward maintaining physiological NADPH homeostasis, which is regulated by glucose-6-phosphate dehydrogenase (G6PD) and AMP kinase (AMPK)[8]. Intriguingly, the physiological steroid hormone dehydroepiandrosterone (DHEA), a well-known G6PD inhibitor that is thought to inhibit NADPH regeneration, actually activated the AMPK pathway, rerouted NADPH utilization from reductive biosynthesis to antioxidant functions, and showed pro-survival effects in the glucose-fed state under oxidative stress through the maintenance of NADPH levels. We further demonstrated that the iNap sensors can be used to report NADPH fluctuations during the activation of macrophages or during the wound response *in vivo*.

Protocol overview.—In this protocol, we describe strategies for *in situ* multiplex fluorescence imaging of pyridine nucleotides, thiol redox and H_2O_2 using genetically encoded sensors in single cells. The procedure consists of 4 key stages. The first section of the protocol describes protein expression, purification and titration of iNap sensors (Steps 1–4). According to the affinities (from the titration data) of iNap1–4, researchers could choose appropriate iNap sensor for their applications in different cells (e.g., *E.coli*, yeast, mammalian) or organelles. Furthermore, researchers also could use the recombinant iNap protein for intracellular NADPH quantification (Please refer to a SoNar-based protocol for quantification of intracellular NADH/NAD^+ redox state[23]). The second section describes the steps used for three-parametric (Fig. 3a) or four-parametric imaging (Fig. 4a), and long-term imaging (Fig. 5a) of redox sensors in single cells. The third section of the protocol (Steps 12–17) describes the flow cytometry analysis of redox sensors in living cells (Fig. 6). The fourth section of the protocol (Steps 18–32) describes the steps for the preparation of sensor mRNA, microinjection and multi-parametric imaging of zebrafish expressing redox sensors (Fig. 7).

Throughout this protocol, NADPH and NADH sensors with green fluorescent spectra are used (i.e., iNap and SoNar), and the thiol redox and H_2O_2 sensors excited and imaged in the red (i.e., rxRFP and HyPerRed) or green (i.e., roGFP1 and HyPer) fluorescent channels. With these tools, researchers can easily obtain comprehensive redox information at the single cell and subcellular levels by multi-location or multi-color imaging of sensors.

Advantages and applications of the approach.—NADH/NAD^+, NADPH/$NADP^+$, thiol redox, and H_2O_2 converge to alter core cellular metabolism and perform important closely related roles in the generation of bioenergy (i.e., ATP), biosynthesis of macromolecules, and maintenance of cellular redox status (Fig. 1), three basic needs for virtually all organisms. In contrast to traditional biochemical or imaging methods targeting individual redox molecules with fragmented information, multiplex analysis of redox

landscapes and dynamics in living cells and *in vivo* is a powerful and flexible technique for exploring protein/metabolite functions in biological systems and for elucidating dynamic biological processes in which pyridine nucleotides, thiol redox, and H_2O_2 have an integrative role.

The Procedures described in this Protocol can be robustly applied to studies of cell cycle dynamics, macrophage activation, as well as in living zebrafish. In addition, this approach can be adapted to different genetically encoded fluorescent sensors using various analytical platforms, such as fluorescence microscopy, high-content imaging systems, flow cytometry, and microplate readers. Considering the fundamental roles of redox biology in life science, this technique will attract the interest of diverse disciplines, from biochemistry to cell biology to disease pathology.

Limitations of the protocol

It is worth mentioning three concerns that must be considered when such techniques are applied in cells or organisms of interest:

- Currently available sensors are not suitable for simultaneous monitoring of the NADPH and NADH redox state in mitochondria because of their equivalent excitation and emission spectra. To overcome this issue, the NADH sensors Frex or SoNar can be used jointly with the spectrally tunable genetically encoded $NADP^+$ sensor recently reported by Rocheleau's group[38]. These $NADP^+$ sensors, termed Apollo-$NADP^+$, are based on $NADP^+$-induced homodimerization of enzymatically inactive G6PD fused to a fluorescent protein, which induces homoFRET between these fluorescent proteins[38]. Apollo-$NADP^+$ sensors are available in combination with various fluorescent proteins; however, they have a rather small dynamic range (up to 15–20%), and their imaging is heavily dependent on sophisticated instrumentation to measure steady-state fluorescence anisotropy, which is not readily available in most laboratories. In practice, the fluorescent response range of the Apollo-$NADP^+$ sensor in live cells under oxidative stress may be 5% or less, making determination of the NADPH/$NADP^+$ redox state rather challenging. Therefore, the development of a highly responsive, red sensor for NADPH or $NADP^+$ visualization in living cells remains highly desirable.
- Unlike the NADH/NAD^+ ratio sensor SoNar, the iNap sensors will not permit the measurement of the NADPH/$NADP^+$ ratio, which is more physiologically relevant than the free concentration of NADPH. In cells, the level of free NADPH is estimated to be much higher than that of free $NADP^+$ [9,31,39] (Table 2). Considering that total NADPH and $NADP^+$ pools are usually stably maintained, thus, a small change in NADPH level is relatively bigger for $NADP^+$ level therefore will largely affect the NADPH/$NADP^+$ ratio. Ideally, of course, a highly responsive and pure NADPH/$NADP^+$ ratio sensor is desirable for measuring intracellular redox state and studying relevant biological processes. Once obtained, it may be used together with the iNap sensors and Apollo-NADP

$^{+}$ to measure all three critical parameters simultaneously, i.e., NADPH, $NADP^{+}$, and their ratio in the cells.

- Compared to pH-resistant roGFP1, Peredox, Grx1-roGFP2, roGFP2-Orp1, roGFP2-Tsa2ΔCR sensors, the fluorescence signals of circularly permuted yellow fluorescent protein (cpYFP)-based iNap, SoNar, Frex, and HyPer sensors (when excited at 488 nm) or rxRFP and HyPerRed sensors (when excited at 561 nm) are highly pH sensitive (Table 1). Thus, pH effects should be carefully considered when these sensors are applied to redox research. In the cytosol, pH effects were generally not observed in studies of cpYFP-based sensors[18,22,24]. For mitochondria, pH-correction is often necessary because the pH is labile depending on the state of energy metabolism and ROS generation. When pH fluctuations occur, they may be corrected by measuring the fluorescence of the redox sensor and its control sensor in parallel. Typically, iNapc, cpYFP and pHRFP are the pH-control sensor of iNap1–4/SoNar, Frex/HyPer and rxRFP/rxRFP1.1, respectively. Taking iNap sensors as an example, the users could calculate the pH-corrected ratio (R'_{iNap}) of cells using the equation:

$$R'_{iNap} = R_{iNap}/R_{iNapc} \quad \text{(Eq. 1)}$$

In this equation, R_{iNap} and R_{iNapc} represent the excitation ratio 420/485 nm for iNap and iNapc, respectively, owing to their very similar pH responses[8]. Alternatively, iNap fluorescence can be measured with pH-resistant 420 nm excitation only, but at the expense of a reduced dynamic range. For ratiometric and pH-resistant measurements, iNap may also be fused to a red fluorescent protein such as mCherry, and measured based on the green/red fluorescence ratio (i.e., 420/590 nm ratio).

Experimental design

Imaging and monitoring multiple redox parameters in single living cells.—The iNap cDNA can be easily delivered to a wide range of cell types by plasmid transfection or lentivirus infection. Here, we used a HeLa cell line co-expressing different redox sensors that were delivered using a liposomal transfection reagent. For multi-parametric imaging of single cells, optimization of the proportion of sensor plasmids is a critical step following their co-transfection into cells. This step not only determines whether “positive” cells are expressing all sensors in a single cell but also determines whether the fluorescence intensity of each sensor is comparable. Dual-excitation ratios are acquired using a Leica TCS SP8 SMD confocal laser scanning microscope system with super-sensitive HyD hybrid detectors. For simultaneous imaging of multi-parameters, we suggest that researchers first focus on mitochondria. High axial resolution imaging of mitochondria may be obtained with a smaller pinhole. Shorter exposure times are generally helpful for reducing photobleaching and phototoxicity. For real-time imaging during the cell cycle, stable cell lines are highly desirable. Transient transfection usually causes lower cell viability and is not ideal for long-term imaging. Dual-excitation ratio images are acquired using a high-performance fluorescence microscope with the necessary accessories, including a stable light source, a

high-sensitivity CCD camera, appropriate filters, filter wheels, a perfect focus system for real-time imaging, and a CO_2 incubator for long-term imaging.

Flow cytometry analysis of redox landscapes in resting and activated RAW264.7 mouse macrophages.—For exogenous gene delivery using the most common cell lines, many lipid-based transfection reagents can be applied and are also commercially available (i.e., Lipofectamine 2000). For difficult-to-transfect primary cells, lentivirus or adenovirus infection is the preferred means for gene delivery. As professional phagocytes, macrophages are endowed with many potent degradative enzymes that can disrupt nucleic acid integrity and make gene transfer into these cells an inefficient process[40]. In addition, macrophages are very responsive to “danger signals” and have potent anti-viral responses. Therefore, we highly recommend non-liposomal and non-viral transfection approaches for macrophages.

Lipopolysaccharide (LPS) and interferon-γ (IFN-γ) are often used for macrophage activation in which their incubation time is a critical step. In general, an 8-h incubation is necessary, and 14–16 h is better. For high-throughput analysis, flow cytometry with a 96-well plate holder is more efficient. Macrophages display obvious metabolic reprogramming during activation, from low glycolysis (M0 macrophages) to high glycolysis (M1 macrophages)[41]. Owing to lactate production, a control sensor is recommended for correcting pH effects, especially cpYFP-based redox sensors.

Multi-parametric imaging of redox sensors in living zebrafish.—For *in vivo* imaging in zebrafish embryos, six important aspects must be considered in the experimental design: (1) sterile and high-quality mRNA; (2) one-cell-stage zebrafish embryos with high viability (generally, low-viability embryos are prone to death after microinjection); (3) the amount and ratio of mRNA for each sensor when performing multi-parametric imaging; (4) expression time of the sensor after mRNA microinjection (typically 48 h); (5) optimization of anesthetic dosage (overdose easily causes the death of zebrafish larvae); (6) Zebrafish larvae pigment commences at approximately 24 hours post fertilization[42]. Thus, if necessary (e.g. 24–72 hr postfertilization larvae imaging), a melanization inhibitor (such as N-phenylthiourea (PTU)) should be added to egg water to prevent pigment formation and avoid the interference of autofluorescence from pigments. Dual-excitation ratios are acquired using a Leica TCS SP8 SMD confocal laser scanning microscope system with super-sensitive HyD hybrid detectors and a HC Plan Fluotar 5×/0.15 NA objective.

MATERIALS

REAGENTS

Δ CRITICAL The indicated reagents and suppliers listed below can be substituted by appropriate alternatives if necessary.

- Cells of interest: we used: HeLa human cervical carcinoma cells (Cell Bank of Chinese Academy of Science, cat. no. TCHu 187), RAW264.7 murine macrophages (Cell Bank of Chinese Academy of Science, cat. no. TCM13), HEK293T human embryonic kidney epithelial cells (Cell Bank of Chinese

Academy of Science, cat. no. GNHu17). **! CAUTION** All cell lines should be regularly checked to ensure that they are authentic and not infected with *Mycoplasma*.

- One-cell-stage zebrafish embryos and 2-d zebrafish larvae. **! CAUTION** The handling procedures were approved by the Institute of Biochemistry and Cell Biology, Chinese Academy of Sciences. Any experiments involving live zebrafish must conform to relevant institutional and national regulations.
- JM109 (DE3) chemically competent cells (Yeasen, cat. no. 11807ES80)
- DMEM (HyClone, cat. no. SH30243.01)
- RPMI 1640 medium (HyClone, cat. no. SH30809.01B)
- Fetal bovine serum (Gibco, cat. no. 10270-106)
- Phenol red-free DMEM (Gibco, cat. no. 21063029)
- Penicillin-streptomycin solution (HyClone, cat. no. SV30010)
- 0.25% (wt/vol) trypsin-EDTA (Gibco, cat. no. 25200-072)
- Hieff Trans liposomal transfection reagent (Yeasen, cat. no. 40802ES03)
- FuGENE HD transfection reagent (Promega, cat. no. E2311)
- Opti-MEM I reduced-serum medium (Invitrogen, cat. no. 31985-070)
- DPBS (HyClone, cat. no. SH30013.04)
- D-glucose (Sigma, cat. no. G7021)
- Poly-brene (Sigma, cat.no. H9268)
- DMSO (Sigma, cat. no. D2650)
- Instant ocean sea salts (Aquarium Systems, cat. no. SS15-10)
- Lithium chloride (Aladdin, cat. no. L116326)
- EDTA (Sigma, cat. no. EDS)
- Poly-D-lysine (Yeasen, cat.no. 40119ES10)
- Puromycin (Yeasen, cat.no. 60210ES25)
- Isopropyl-β-D-thiogalactoside (Yeasen, cat. no. 10902ES08)
- Tryptone (Oxoid, cat. no.LP0042)
- Yeast extract (Oxoid, cat. no.LP0021)
- Ampicillin (Yeasen, cat. no. 60203ES10)
- Na_3PO_4 (Sigma, cat. no. 342483)
- NaCl (Sigma, cat. no. 746398)
- Imidazole (Sigma, cat. no. 576166)

- HEPES (Vetec, cat. no. V900477)
- KCl (Shanghai Titan Scientific Co., Ltd., cat. no. G80636B)
- KH_2PO_4 (Vetec, cat. no. V900041)
- $Na_2HPO_4 \cdot 12\ H_2O$ (Shanghai Titan Scientific Co., Ltd., cat. no. G10267A)
- $MgSO_4$ (Vetec, cat. no. V900066)
- $CaCl_2$ (Vetec, cat. no. V900266)
- $NaHCO_3$ (Vetec, cat. no. V900182)
- PrimeSTAR MAX DNA polymerase (Takara, cat. no. R045A)
- SP6 Primer (Generay)
- SV40 Poly(A) Primer (Generay)
- BSA, bovine serum albumin (Yeasen, cat. no. 36101ES60)
- BCA protein quantification kit (Yeasen, cat. no. 20201ES76)
- SanPrep column DNA gel extraction kit (Sangon Biotech, cat. no. B518131)
- mMESSAGE mMACHINE kit (Invitrogen, cat. no. AM1340)
- Agarose (Yeason, cat. no. 10208ES60)
- NADPH (Yeason, cat. no. 60302ES01)
- IFN-γ, recombinant mouse interferon γ (Absin, cat. no. abs01021d)
- LPS, lipopolysaccharides from *Escherichia coli* (Yeasen, cat. no. 60322ES10)
- Tricaine (Sigma, cat. no. A5040). **! CAUTION** Tricaine is an anesthetic for zebrafish. Wear gloves, a mask, safety glasses and a laboratory coat when handling tricaine.
- N-phenylthiourea (Sigma, cat. no. P7629)
- Sodium oxamate (Sigma, cat. no. O2751) **! CAUTION** Sodium oxamate is an inhibitor of glycolysis. Wear gloves, a mask, safety glasses and a lab coat when handling sodium oxamate.
- Rotenone (Sigma, cat. no. R8875). **! CAUTION** Rotenone is a potent inhibitor of mitochondrial complex I. Wear gloves, a mask, safety glasses and a lab coat when handling rotenone.
- Diamide (Sigma, cat. no. D3648). **! CAUTION** Diamide is a thiol oxidizing agent. Wear gloves, a mask, safety glasses and a lab coat when handling diamide.
- H_2O_2 (Sigma, cat. no. 216763). **Δ CRITICAL** store at 4°C for up to one year. **! CAUTION** H_2O_2 is an oxidizing agent. Wear gloves, a mask, safety glasses and a lab coat when handling H_2O_2.
- Plasmids: see Table 3

EQUIPMENT

- Leica confocal microscope with TCS SP8 SMD system (Leica)
- SZX10 stereoscopic microscope (Olympus)
- Eclipse Ti-E automatic microscope (Nikon)
- Cooled monochrome digital microscope camera DS-Qi1 (Nikon)
- Lambda XL light source (Sutter Instrument)
- Lambda 10–3 filter wheel (Sutter Instrument)
- CO_2 incubator (Tokai Hit)
- Filter sets for microscope imaging (407 BP 17 nm and 482 BP 35 nm from Semrock, and 535 BP 40 nm from Omega Optical)
- CytoFLEX S flow cytometer (Beckman Coulter)
- FACS Aria I flow cytometer (BD Biosciences)
- Countstar IC1000 automated cell counter (Isogen Life Science)
- Pneumatic microinjector (Narishige, IM-300)
- Joystick micromanipulator (Narishige, MN-151)
- Injection holder (Narishige, HI-7)
- Glass capillaries (Narishige, G-1)
- Treadlite II foot operated switch (Linemaster, T-91-S)
- Micropipette ruller (Sutter Instrument, P-97)
- Synergy 2 multi-mode microplate reader (BioTek)
- Nucleic acid electrophoresis (PowerBC, 3002SI)
- PCR instrument (Biometra, TOne 96G)
- Ultra-violet ray lamp box (Tanon, UV-2000)
- NTA column (GE healthcare, 17531804)
- a prepacked column with Sephadex® G-25 Medium (GE healthcare, 17003301)
- pH meter (Bante, PHS-3BW)
- 0.22 μm filter membrane (Millipore, SLGP033RS)
- 35 mm glass-bottom dish (In Vitro Scientific, D35C4–20-1-N)
- 96-well glass-bottom plate (In Vitro Scientific, P96-10-0-N)
- Black 96-well flat-bottom plate (WHB, 96-02)
- Eight-channel 1.2 ml electronic pipette (Eppendorf)
- 10 μl, 50 μl, 200 μl, 1000 μl manual pipette (Biohit)

- 1.5-ml nuclease-free Eppendorf tube (Invitrogen, AM12400)
- ImageJ software (ImageJ 1.50d, https://imagej.nih.gov/ij/)
- FlowJo software (https://www.flowjo.com/solutions/flowjo)

REAGENT SETUP

Δ CRITICAL All buffers should be sterilized using a 0.22 μm filter membrane.

Cloning strategies for plasmids iNap, iNapc, SoNar, Frex, rxRFP, roGFP1, HyPerRed, HyPer, pHRFP, cpYFP The entire coding sequence of iNap1–4 was subcloned into the pRSETB vector (Invitrogen) for prokaryotic expression; the entire coding sequence of iNap1/3, iNapc, SoNar, Frex, rxRFP, HyPerRed, HyPer, pHRFP, or cpYFP with or without signal peptides was subcloned into the pcDNA3.1/Hygro$^{(+)}$ vector (Invitrogen) for mammalian expression; the entire coding sequence of iNap1, iNapc, SoNar, roGFP1, or HyPer without signal peptides was subcloned into pLVX-IRES-Puro vector (Clontech) for generating recombinant lentivirus; and the entire coding sequence of iNap1, iNapc, SoNar, or HyPerRed without signal peptides was subcloned into the pTol2 vector for mRNA transcription. For nuclear, nuclear-excluded, or mitochondrial targeting, the localization sequences were inserted at the C-terminus or N-terminus of sensors as previously described[8,22,24]. All constructs, including iNap1–4, iNapc, SoNar, Frex, and cpYFP (see Table 3), are available upon request.

Δ CRITICAL All of the sensors described in this protocol express well in mammalian cells and *E. coli*, making it unnecessary for researchers to perform codon optimization for expression of sensors in these cells. For expression in other cell types, such as yeast cells, these sensors may require codon optimization, which can be performed using Gene Designer 2.0 software (DNA 2.0)[44].

HeLa cell culture medium: DMEM supplemented with 10% fetal bovine serum and 1% penicillin-streptomycin. Store at 4°C for up to one month and pre-heat to 37°C before use.

RAW264.7 cell culture medium: RPMI 1640 medium supplemented with 10% fetal bovine serum and 1% penicillin-streptomycin. Store at 4°C for up to one month and pre-heat to 37°C before use.

PBS containing 25 mM glucose (PBS-G): 20 mM HEPES, 2.7 mM KCl, 138 mM NaCl, 1.5 mM KH_2PO_4, 8.1 mM Na_2HPO_4, 25 mM D-glucose, pH 7.4. Prepare sterilized PBS by autoclaving and sterilized glucose stocking solution by filtering. **Δ CRITICAL** Store at 4°C for up to one month and pre-heat to 37°C before use.

HBSS containing 10 mM HEPES (pH 7.4): 10 mM HEPES, 5.4 mM KCl, 136.7 mM NaCl, 0.44 mM KH_2PO_4, 0.35 mM Na_2HPO_4, 0.81 mM $MgSO_4$, 1.26 mM $CaCl_2$, 4.2 mM $NaHCO_3$. Adjust the pH to 7.4 with 4 M NaOH. **Δ CRITICAL** Store at 4°C for up to one month and pre-heat to 37°C before use.

PBS containing 0.1% (wt/vol) BSA (PBS-B): 20 mM HEPES, 2.7 mM KCl, 138 mM NaCl, 1.5 mM KH_2PO_4, 8.1 mM Na_2HPO_4, 0.1% (wt/vol) BSA, pH 7.4. Prepare fresh.

Buffer A: 20 mM sodium phosphate, 500 mM sodium chloride, and 10 mM imidazole, pH 7.4. Prepare fresh.

Buffer B: 20 mM sodium phosphate, 500 mM sodium chloride, and 300 mM imidazole, pH 7.4. Prepare fresh.

E3 medium: E3 medium containing 5 mM NaCl, 0.17 mM KCl, 0.33 mM $CaCl_2$, and 0.33 mM $MgSO_4$. Store at 4°C for up to one month.

Egg water: Dissolve 60 mg Instant Ocean Sea Salts to 1 L distilled water. Store at 4°C for no more than one month.

LiCl precipitation solution: 7.5 M lithium chloride, 50 mM EDTA, pH 8.0. Store at −20°C for no more than one year.

LB: 10 g sodium chloride, 10 g tryptone and 5 g yeast extract were dissolved in 1 L ddH_2O. Prepare fresh and sterilized LB by autoclaving.

Ampicillin (100 mg/ml): Dissolve 5 g ampicillin in 50 ml ddH_2O. Store in small aliquots at −20°C for up to six months.

NADPH: NADPH stock solution (100 mM) was made by dissolving the NADPH powder into HEPES buffer containing 100 mM NaCl (pH 7.3). **Δ CRITICAL** Prepare fresh and wrap the container with aluminum foil.

Recombinant mouse interferon γ (IFN-γ): Dissolve the IFN-γ powder into PBS-B to a stock concentration of 100,000 U/ml. Store the solution in small aliquots at −20°C for up to one month.

Lipopolysaccharides from *Escherichia coli* (LPS): Dissolve the LPS powder into double-distilled water to a stock concentration of 2 mg/ml. Store the solution in small aliquots at −20°C for up to one month.

N-phenylthiourea: Prepare the N-phenylthiourea stock solution (100 mM) by dissolving the N-phenylthiourea powder into DMSO. Store it at −20°C for up to one month.

Tricaine: Dissolve 500 mg tricaine powder in 5 ml water to a final concentration of 100 mg/ml. Store at 4°C for up to one week.

Oxamate: Prepare the oxamate stock solution (200 mM) by dissolving oxamate powder in PBS-G. Prepare fresh.

Pyruvate: Dilute the pyruvate stock solution with PBS-G to make a series of working solutions: 10–1000 μM. Prepare fresh.

Rotenone: Prepare the rotenone stock solution (10 mM) by dissolving the rotenone powder in DMSO. Store at at −20°C for up to six months. Dilute in PBS-G before use.

Diamide: Prepare the diamide stock solution (200 mM) by dissolving diamide powder into DMSO. Store at −20°C for up to one month. Dilute in PBS before use.

H_2O_2: Dilute the 30% (wt/vol) stock solution in PBS directly before use.

EQUIPMENT SETUP

Leica TCS SP8 confocal laser scanning microscope system—The Leica confocal microscope with the TCS SP8 system includes the following parts: inverted microscope Leica DMI6000 equipped with super-sensitive HyD hybrid detectors, HC Plan Fluotar 5×/0.15 NA objective, HC Plan Apo CS 40×/0.85 NA objective and HC Plan Apo CS2 63×/1.40 NA oil objective, anti-vibration table, image-based autofocus for transmission light combined with adaptive focus control (AFC), lasers (diode, 50 mW: 405 nm; Ar 65 mW: 488 nm; DPSS, 20 mW: 561 nm), PMT detection for imaging, fluorescence lamp EL6000, and software platform Leica Application Suite X (LAS X).

High-performance fluorescence microscopy system—The fluorescence microscopy system is equipped with a Nikon Eclipse Ti-E automatic microscope, monochrome-cooled digital microscope camera DS-Qi1 Mc-U2, perfect focus system (PFS), A Plan Apo 40×0.95 NA objective, highly stable Sutter Lambda XL light source, and on-stage CO_2 incubator (Tokai Hit). For dual-excitation ratio imaging, 407 BP 17 nm or 482 BP 35-nm bandpass excitation filters (Semrock) and a 535 BP 40-nm emission filter altered by a Lambda 10–3 filter wheel (Sutter Instruments) were used[23].

Fluorescence-activated cell sorter analysis (FACS)—The CytoFLEX S Flow Cytometer is equipped with four spatially separated lasers: violet laser (405 nm), blue laser (488 nm), yellow laser (561 nm), and red laser (638 nm), with up to 13 fluorescent channels. The CytoFLEX system includes a 96-well plate loader and is compatible with high-throughput assays. Forward scatter detection is based on the proprietary axial light loss sensor system using silicon photodiodes with a built-in 488/8 nm band-pass filter. Fiber optics are used to deliver fluorescence and side scatter light to Avalanche Photo Diode detector arrays. For signal processing, a fully digital system with 7-decade data display is used. Emission profile acquisition relies on reflective optics and single transmission band-pass filters (KO525, 525/40 nm; FITC, 525/40 nm). Sample flow rates can be adjusted from 10 to 240 μl/min in 1-μl increments depending on the cell density. The 96-well standard flat, U or V bottom plates are all available for the equipment.

Zebrafish microinjection system—The zebrafish microinjection system includes a Narishige IM-300 microinjector, MN-151 Joystick micromanipulator, Olympus SZX10 stereoscopic microscope, Linemaster treadlite II foot-operated switch, and other necessary accessories: HI-7 injection holder, G1 glass capillary. Nitrogen serves as the gas power supply, and its pressure is controlled between 40–50 psi. The IM 300 microinjector serves as the main module of the system and connects the micromanipulator and foot-operated switch. The HI-7 injection holder is designed for the G1 Glass capillary, and the two parts are placed on the MN-151 Joystick micromanipulator. The IM 300 microinjector is a multi-functional, electrically controlled pneumatic injector for the precise control of small volumes. Injection

volumes are variable from microliters to femtoliters. Each zebrafish embryo is injected with 1 nl mRNA through glass capillaries.

PROCEDURE

Protein expression, purification and titration of iNap sensors ● TIMING 3 d—

1| Culture *E. coli* JM109 (DE3) cells carrying pRSETB-iNap in 100 ml LB medium containing 0.1 mg/ml ampicillin at 37°C, and induce protein expression in the recombinant bacteria at an approximate OD_{600} of 0.4–0.6 with 1 mM isopropyl-β-D-thiogalactoside (IPTG) at 18°C for 30 h.

Δ CRITICAL STEP The OD_{600} values must be between 0.4 and 0.6; otherwise, it will be difficult to express the protein.

? TROUBLESHOOTING

2| Harvest bacteria by centrifugation at 1,500 g for 20 min at 4°C, suspend the cell pellet in 25 ml Buffer A. Set time of sonication, cycles and percent amplitude as 300 s (1 s sonication, 3 s rest period), 4, and 45%, and then lyse the cells by sonication.

Δ CRITICAL STEP Cell pellets should be thoroughly sonicated.

3| Purify proteins using an NTA column (GE Healthcare). Wash the column with 10 ml Buffer A containing 50 mM imidazole, and then elute the proteins with 5 ml Buffer B. Desalt the protein preparations using a prepacked column with Sephadex® G-25 Medium and exchange it into 100 mM HEPES buffer containing 100 mM NaCl (pH 7.3) for *in vitro* characterization.

■ **PAUSE POINT** The purified protein can be stored at −80°C for analysis at a later time point.

4| For nucleotide titration experiments, prepare a 100 mM NADPH stock solution in HEPES buffer containing 100 mM NaCl (pH 7.3). Perform each assay by combining 50 μl of the NADPH working solution (0–20 mM) and 50 μl sensor protein (0.4 μM) in a black 96-well flat bottom plate. Measure the fluorescence intensity after addition of iNap using a filter-based Synergy 2 Multi-Mode microplate reader with 420 BP 10 nm or 485 BP 20 nm excitation and 528 BP 20 nm emission bandpass filters.

Δ CRITICAL STEP For the titration experiments, a sensor concentrations as low as possible (i.e., 0.1 μM or 0.2 μM) must be used to obtain accurate binding and dissociation constants. High sensor concentrations lead to overestimation of the affinity of sensors in the titration experiments.

Δ CRITICAL STEP Read the fluorescence immediately after addition of the sensor protein.

Multi-parametric imaging of redox landscapes and dynamics in single cells ● TIMING 2–3 d—

5| Coat the 96-well glass bottom plate with 0.1 mg/ml poly-D-lysine (PDL) at 37°C for at least 3 h. Remove the coating reagents and wash twice with 100 μl

PBS. Seed cells of interest in the plate at 20–30% confluency. Grow the cells overnight at 37°C, 5% CO_2.

Δ CRITICAL STEP Alternatively, the imaging plates or dishes can be coated with fibronectin, collagen I, collagen IV, laminin or fibrinogen depending on the cell type[45,46], to avoid cell detachment.

Δ CRITICAL STEP Cells are expected to be 30–50% confluent at the time of transfection on the next day. Transfecting cells at a lower density allows a longer expression time for gene delivery, and minimizes the loss of cell viability due to cell overgrowth.

? TROUBLESHOOTING

6| Deliver multiple sensor-expressing plasmids into cells by combining the coding plasmids in the following molar ratios. For three-parametric imaging:

Nes-iNap1 : Nuc-SoNar : Cyt-rxRFP (3:1:1)

Mit-iNap3 : Nuc-SoNar : Mit-rxRFP1.1 (3:1:1)

Mit-iNapc : Nuc-iNapc : Mit-pHRFP (1:1:1)

For four-parametric imaging:

Mit-iNap3 : Nuc-SoNar : Mit-rxRFP1.1 : Nuc-HyPerRed (2:1:1:2)

Fix the total amount of plasmids (0.1 μg/well) and the volume of Hieff Trans liposomal transfection reagent (0.3 μl/well), and follow the manufacturer's protocol for detailed transfection.

Δ CRITICAL STEP The ratio between the different sensor-encoding plasmids should be corrected for the differences in mass between the plasmids.

Δ CRITICAL STEP Optimization of the molar ratio of transfected sensor plasmids is crucial. This does not only determine whether all desired sensors are expressed in a single cell but also determines whether the fluorescence intensity of each sensor is comparable during imaging. In principle, we use higher amounts for low-expression sensors, and lower amounts for high-expression sensors. We have added the recommended sensor ratios, so that all desired sensors are appropriately expressed.

Δ CRITICAL STEP Typically, we suggest that researchers use iNapc, and pHRFP as the control sensor of iNap1,3/SoNar, and rxRFP/rxRFP1.1, respectively.

Δ CRITICAL STEP Maintenance of cell viability is essential for assessing the redox state in living cells. Optimization of the transfection conditions, replacement with fresh medium at 4–6 h post-transfection, or choosing transfection reagents with low toxicity (i.e., Fugene HD) can help to reduce cell damage during gene delivery.

Δ CRITICAL STEP For long-term imaging, we recommend making stable cell-lines using lentiviral infection. In short, produce lentivirus by co-transfecting pLVX-sensor vector and two lentiviral packaging vectors (pMD2.G and psPAX2) in HEK293T cells. After infection, select cells with 0.2–1 μg/ml puromycin for 1 week and then sort the fluorescent cells by FACS Aria I. For lentivirus production, please refer to the detailed protocol from Addgene (http://www.addgene.org/protocols/lentivirus-production/) and Tiscornia, G., et. al.[47] For lentivirus infection, target cells in 6-well tissue culture plates are infected in media containing 8 μg/ml of polybrene and centrifuge at 1,000 g for 1 hr.

7| Incubate the cells at 37°C in a humidified atmosphere using a CO_2 incubator. After 24–36 h, remove the medium, rinse cells twice with 100 μl PBS-G, and then add 100 μl PBS-G to each well for imaging.

Δ CRITICAL STEP It is necessary to pre-warm the PBS-G to 37°C. The cell density is expected to reach 70–80% confluency before imaging. All operations must be performed carefully to avoid dislodging the cells from the glass surface.

8| Incubate cells at 37°C for 10–20 min.

9| Open the adaptive focus control (AFC), choose 2–3 moderately fluorescent cells, and record their coordinates. Capture the fluorescence images of iNap1, SoNar, or iNapc using a 40× or 63× oil detection objective, 405 nm or 488 nm excitation laser, and 500–550 nm emission range. Obtain the HyPerRed or rxRFP signals using a 561 nm excitation laser and 570–630 nm emission range.

Δ CRITICAL STEP It is important to obtain a stable baseline ratio before treatment.

Δ CRITICAL STEP We use a Leica TCS SP8 SMD confocal laser scanning microscope system with super-sensitive HyD hybrid detectors (see Equipment Setup).

Δ CRITICAL STEP Optimize the imaging parameters (i.e., laser power, exposure time, and time intervals) to reduce photobleaching and phototoxicity. Although photobleaching and phototoxicity are not often main concerns for fluorescent protein-based sensors, we still suggest that researchers optimize the imaging parameters to reduce such undesired effects.

Δ CRITICAL STEP For long-term imaging (e.g. imaging of cell cycle dynamics), extra care should be taken to optimize the imaging parameters to reduce phototoxicity (i.e., light intensity, exposure time, gain, and time intervals). We acquire dynamic images using a high-performance fluorescence microscopy system equipped with a Nikon Eclipse Ti-E automatic microscope (see Equipment Setup). Open the perfect focus system and choose 2 moderately fluorescent cells. Monitor the sensors for 24 h (time interval: 30 min). Ensure the temperature and CO_2 concentration reach standard requirements during the whole process. Disturbance of temperature or CO_2 concentration would cause undesirable deviations. Check the whole instrument setup every few hours.

? TROUBLESHOOTING

10| (Optional) Add agents to the cell culture media in order to perturb cellular redox state, mix gently, and continue imaging.

Δ CRITICAL STEP Pipette carefully without touching the plate.

11| Export the raw data to ImageJ software as 12-bit TIFs for single-excitation and dual-excitation ratio image analysis. Fluorescence images with 561 nm excitation are pseudocolored red. The image of the excitation ratio of 405/488 nm is determined pixel by pixel and pseudocolored using the Hue-Saturation-Brightness (HSB) color space. Briefly, the red, green, and blue (RGB) values (255, 0, 255) represent the lowest ratios and red values (255, 0, 0) represent the highest ratio, while the color brightness is proportional to the fluorescent signals in both channels.

Flow cytometry analysis of the redox state in resting and activated mouse macrophages ● TIMING 2–3 d—12| Seed RAW264.7 cells in a 12-well plate with a density of 2.5×10^5 cells/well and culture overnight. Deliver sensors into cells with FuGENE HD transfection reagent according to the manufacturer's instructions.

Δ CRITICAL STEP See Step 6 for recommendations on the plasmid ratios. Optimize the transfection conditions and avoid cell damage.

Δ CRITICAL STEP Liposomal transfection and virus infection is not suitable for gene delivery of macrophages. FuGENE HD is a nonliposomal transfection reagent and can deliver DNA into RAW264.7 cells with high efficiency and low toxicity.

Δ CRITICAL STEP During transfection, we suggest that researchers use iNapc-Cyt, cpYFP-Cyt, iNapc-Mit, and cpYFP-Mit as the control sensor of iNap1-Cyt/SoNar-Cyt, HyPer-Cyt, iNap3-Mit, and Frex-Mit/HyPer-Mit, respectively.

? TROUBLESHOOTING

13| Remove the culture medium 12 h after transfection and add fresh medium containing LPS (0.5 μg/ml) plus IFN-γ (250 U/ml) to activate macrophages for 14–16 h.

Δ CRITICAL STEP The incubation time of LPS plus IFN-γ is critical, generally at least 8 h.

14| Remove the medium, rinse the cells twice with PBS, and then add 0.4–0.5 ml HBSS with 10 mM HEPES, pH 7.4, to each well. Scrape the cells gently with a cell lifter and pipette the cells repeatedly to obtain a single cell suspension. Immediately transfer 0.3 ml cell suspension to a 96-well plate for analysis.

Δ CRITICAL STEP The PBS and HBSS should be preheated in a water bath to 37°C before use to maintain cell viability.

15| Measure fluorescence with a flow cytometer. Excite cells with laser lines at 405 nm and 488 nm, and set emission filters 525/40 nm for both excitation wavelengths.

Δ CRITICAL STEP Optimize the measurement parameters in advance—i.e., stabilized lasers, gain value for each channel, and sample flow rate. The total number of recorded events depends on the transfection efficiency, and, thus, it is beneficial to record more fluorescent cells.

16| ***Data acquisition (Steps 16–17):*** Create two dual-parametric dot plots, one with FSC-A (linear) on the x-axis and SSC-A on the y-axis (linear), and the other with KO525-A (log) on the Y-axis and FITC-A (log) on the x-axis. The numerical analysis of all cells and positive cells (sensor-expressing cells) is included in supplementary Table 1.

Δ CRITICAL STEP Dead cells always have a higher side scatter and lower forward scatter than living cells, and, thus, a gate can be set based on FSC versus SSC to analyze viable cells.

Δ CRITICAL STEP In the plot of KO525 (Ex. 405 nm, emission filter set: 525/40 nm) versus FITC (Ex. 488 nm, emission filter set: 525/40 nm), create a quadrant marker to discriminate negative or positive cell populations. Example gating strategy for FSC/SSC and negative cells/positive cells is included in supplementary Fig. 3.

17| Obtain mean fluorescent values of the positive gate using FlowJo software, and calculate the 405/488 nm ratio of cells expressing sensors or pH control sensors, respectively. Calculate the pH-corrected ratio ($R'_{\text{redox sensor}}$) of cells as follows: $R'_{\text{redox sensor}} = R_{\text{redox sensor}}/R_{\text{pH-control sensor}}$ ($R_{\text{redox sensor}}$ and $R_{\text{pH-control sensor}}$ represent the 405/488 nm excitation ratio, respectively)

Δ CRITICAL STEP Macrophages have obvious metabolic reprogramming during activation and produce large amounts of lactate; therefore, pH correction is highly recommended, especially when using cpYFP-based redox sensors.

Spatiotemporal imaging of NADPH, NADH and H_2O_2 in living zebrafish ● TIMING 3 d—! CAUTION

All handling procedures involving live zebrafish must conform to governmental and institutional guidelines and regulations.

18| ***Preparation of sensor mRNA (Steps 18–24):*** Amplify linear template DNA of the pTol2-iNap1, pTol2-SoNar, pTol2-iNapc, and pTol2-HyPerRed vectors by PrimeSTAR MAX DNA polymerase by preparing the following mixture:

Component	Amount (per reaction, μl)	Final
DNA	0.5	25–50 ng
Forward primer[a]	1	5 pmol
Reverse primer[b]	1	5 pmol
PrimeSTAR Max Premix (2×)	12.5	1×
Water	10	10 μl
Total	25	

[a] Forward primer sequences (SP6 promoter): CCATGATTACGCCAAGCTATTTAG

[b], Reverse primer sequences (SV40 poly(A) terminator): CGCTTACAATTTACGCCTTAAGATAC

Run the PCR programs as follows:

Cycle number	Denature	Anneal	Extend
1–30	98°C, 5 min	55°C, 15 s	72°C, 10s (5 s / kb)

Δ CRITICAL STEP The extension time depends on the length of DNA fragments.

19| Obtain the DNA fragments via electrophoresis and gel extraction, quantify the DNA and prepare for *in vitro* mRNA transcription.

Δ CRITICAL STEP The quality of DNA is vital for *in vitro* mRNA transcription.

20| According to the manufacturer's manual (mMESSAGE mMACHINE kit), assemble transcription reactions at room temperature (20–25°C) to the final volume 20 μl in nuclease-free Eppendorf tube. Mix gently and incubate at 37°C for 2 h.

Δ CRITICAL STEP Use of nuclease-free water or disposables (e.g. pipette tips) is essential in step 20 and all further steps, in which mRNA is manipulated.

21| Add 1 μl TURBO DNase, mix gently and incubate at 37°C for 15 min to remove the template DNA.

Δ CRITICAL STEP If researchers want to remove the template DNA completely, we recommend performing the DNase treatment. Generally, it may not be necessary to do this because the template DNA will be present at a very low level relative to the transcriptional mRNA.

22| Precipitate the mRNA by adding 30 μl nuclease-free water and 30 μl LiCl precipitation solution (7.5 M). Mix thoroughly and incubate for ≥30 min at −20°C.

Δ CRITICAL STEP Considering that the concentration of LiCl working solution is 2.5–3 M, please do not excessively dilute the transcription reaction with water to avoid low yields of mRNA. For a greater yield of mRNA, incubation for 1 h is more effective.

23| Centrifuge at 4°C for 15 min at 13, 000 g to pellet the mRNA. Carefully remove the supernatant, wash the pellet once with 70% (vol/vol) ethanol, and re-centrifuge to maximize the removal of unincorporated nucleotides.

Δ CRITICAL STEP 70% (vol/vol) ethanol should be made by diluting absolute ethanol into sterile, nuclease-free water.

24| Carefully remove the 70% (vol/vol) ethanol, and resuspend the mRNA in 15 μl nuclease-free water. Determine the RNA concentration.

Δ CRITICAL STEP Ethanol should be thoroughly removed. Removal of ethanol can be improved by using an evaporator ("SpeedVac") to dry the pellet.

Δ CRITICAL STEP Do not overdry the pellet.

Δ CRITICAL STEP Splitting into small aliquots is preferred, as repeated refreezing and thawing may lead to mRNA degradation.

PAUSE POINT The obtained mRNA can be stored at −80°C (up to one month) to be used at a later time point.

25| *Microinjection and culture of zebrafish embryos (Steps 25–29):* Mount the capillary needle in a micromanipulator (see Equipment Setup) and adjust the microinjection apparatus (e.g., injection pressure, injection volume, injection times, etc.). Use micropipette puller to produce the pipette's tip (22–25 μm) from glass capillary (For more detailed instructions, please refer to the operation manual of micropipette puller Model P-97). Cut the needle at an angle (30–45 degrees) to create a beveled tip. Measure the drop size and check that it is 1 nl per injection. For more detailed instructions, please refer to the protocols from Gutzman J.H. and Sive H.(http://www.jove.com/index/Details.stp?ID=1218) and Xu Q.[48]

Δ CRITICAL STEP A microscaler can be used to determine the volume to 1 nl.

26| Coat a 100 mm plastic dish with 25–30 ml 1% (wt/vol) agarose, and poke holes in the agarose-coated dish with a plastic 1–200 μl pipette tip. Carefully remove the agarose plugs from the holes using forceps. Transfer fertilized one-cell-stage zebrafish embryos into the holes and orient them so that the injection apparatus can approach from the posterior side of the embryo.

Δ CRITICAL STEP Fertilized eggs with high viability are important for a high survival rate.

27| Dilute the mRNA from Step 24 to a final concentration of 50 ng/μl, and inject 1 nl it into the fertilized one-cell eggs. For co-imaging of NADH/NAD^+ and H_2O_2 dynamics in zebrafish, mix SoNar and HyPerRed mRNA at a molar ratio of 1:3 and microinject the total mRNA at a final concentration of 300 ng/μl.

Δ CRITICAL STEP The final concentration of mRNA is generally 50 ng/μl for each sensor, and the total amount can be adjusted according to the fluorescence and survival of injected eggs.

Δ CRITICAL STEP mRNA should be kept cold to avoid degradation. To ensure that mRNA is injected into embryos successfully, the mRNA can be mixed with indicator dyes such as phenol red (at the final concentration of 0.05% (wt/vol)).

28| Maintain the embryos in egg water at 28°C for 2 d under standard laboratory conditions.

29| (Optional) After culturing for 24 h, replace the egg water with fresh E3 medium containing 0.1 mM N-phenylthiourea (PTU) to prevent melanin formation.

Δ CRITICAL STEP Melanin can be formed during embryonic development. N-phenylthiourea (PTU) can inhibit melanogenesis by blocking all tyrosinase-dependent steps

in the melanin pathway[42]. Melanin-expressing melanophores are involved in the formation of longitudinal stripes of black in the skin[49,50].

30| *In vivo* imaging of living zebrafish (Steps 30–32): After 2 d, puncture the egg membranes with syringe needles and then transfer the larvae to a 24-well glass-bottom plate, one zebrafish larva per well. Before imaging, anesthetize zebrafish larvae in E3 medium with 0.6 mM tricaine.

Δ CRITICAL STEP Ensure the zebrafish are fully anesthetized to avoid zebrafish twisting or moving during the imaging process. The dosage of anesthetic should be adjusted according to the state of different batches of larvae. To minimize movement, larvae can also be fixed in 1% (wt/vol) low-melting agarose.

31| After 2–3 min, capture fluorescence images of iNap1, SoNar, or iNapc using a 5× objective, 405 nm or 488 nm excitation lasers, and a 500–550 nm emission range. Obtain the HyPerRed signal using a 561 nm excitation laser and 570–630 nm emission range.

? TROUBLESHOOTING

32| Export the raw data to ImageJ software as 12-bit TIFs for single-excitation and dual-excitation ratio image analysis. Fluorescence images with 561 nm excitation are pseudocolored red. The image of the excitation ratio of 405/488 nm is determined pixel by pixel and pseudocolored using the Hue-Saturation-Brightness (HSB) color space. Briefly, the red, green, and blue (RGB) values (255, 0, 255) represent the lowest ratios and red values (255, 0, 0) represent the highest ratio, while the color brightness is proportional to the fluorescent signals in both channels.

TROUBLESHOOTING

Troubleshooting guidance can be found in Table 4.

TIMING

Reagent preparation: 1–2 h

Steps 1–4, protein expression, purification and titration of iNap sensors: 3 d

Steps 5–11, seeding, transfection, three-parametric and four-parametric imaging of redox sensors in single living cells: 2–3 d

Steps 12–13, seeding, transfection, activation of RAW264.7 cells: 2–3 d

Steps 14–17, flow cytometry analysis of redox sensors in living cells: 60 min

Steps 18–24, preparation of sensor mRNA: 5–6 h

Steps 25–29, microinjection and culture of zebrafish embryos: 2–3 d

Steps 30–32, *in vivo* imaging of living zebrafish: 10–60 min

ANTICIPATED RESULTS

This protocol assists researchers in achieving multiplex analysis of redox landscapes and dynamics in living cells and *in vivo*. To measure NADPH, NADH, and thiol redox in single living cells simultaneously, we expressed iNap1 in the cytosol using a nucleus-excluded signal peptide, SoNar in the nucleus using a nuclear localization signal, and rxRFP throughout the whole cell (Fig. 3b, c); alternatively, we expressed iNap3 in the mitochondrial matrix using a mitochondrial signal peptide, SoNar in the nucleus, and rxRFP1.1 in the mitochondrial matrix (Fig. 3d, e). In cells treated with the thiol-specific oxidant diamide, we observed a marked decrease in cytosolic and mitochondrial NADPH and thiol levels, but not nuclear NADH (Fig. 3b, d). In cells treated with the lactate dehydrogenase (LDH) inhibitor oxamate to increase the cytosolic NADH/NAD^+ ratio[22], we observed a marked change in SoNar fluorescence but not in that of iNap1, iNap3, or rxRFP (Fig. 3c, e). Minimal changes in fluorescence were observed in control iNapc and pHRFP-expressing cells with diamide or oxamate treatment (Supplementary Fig. 1a–d), indicating that there is only limited pH variation. To measure NADPH, NADH, thiol redox, and H_2O_2 in single living cells simultaneously, we expressed iNap3 and rxRFP1.1 in the mitochondrial matrix, and SoNar and HyPerRed in the nucleus (Fig. 4b–d). In cells treated with the oxidants diamide and H_2O_2, we observed a marked change in the fluorescence of iNap3, rxRFP1.1 and HyPerRed, but not in that of SoNar (Fig. 4b, c). In contrast, nuclear SoNar showed obvious changes in fluorescence upon oxamate treatment (Fig. 4d).

Metabolic reprogramming and accelerated cell cycle progression are two important hallmarks of cancer cells, while how they are coordinated to promote cancer cell growth is poorly understood. During cell cycle progression, we observed a moderate change in the fluorescence of iNap1, but not that of SoNar, roGFP1, HyPer, or iNapc (Fig. 5b, c and Supplementary Fig. 2a, b), indicating that the increase in cytosolic NADPH plays an essential role during cell division, in agreement with a recent study[51].

Macrophage activation is known to induce drastic metabolic reprogramming. Resting macrophages have low glycolysis rates but high rates of fatty acid oxidation (FAO) and oxidative phosphorylation (OXPHOS)[41]; activated macrophages depend on glycolysis rather than mitochondrial ATP production and release ROS and reactive nitrogen species (including nitric oxide) for killing pathogens[41]. However, a comprehensive evaluation of redox landscapes is lacking in resting and activated macrophages. We further established a biosensor-based flow cytometry analysis. Lipopolysaccharide (LPS) and interferon-γ (IFN-γ) treatment induced a significant increase in NADH in the cytosol and mitochondria (Fig. 8a–d), suggesting mitochondrial inhibition and glycolysis activation in activated macrophages. Furthermore, its activation also induced significant oxidative stress, as shown by NADPH depletion and thiol oxidation in the cytosol and mitochondria, rather than H_2O_2 generation (Fig. 8a–d), consistent with previous reports that macrophages synthesize nitric oxide and consume NADPH upon activation[52]. The $R_{405/488}$ of iNapc or cpYFP increased slightly in activated RAW264.7 macrophages compared with resting cells, which may be explained by the acidification of the cells (Supplementary Fig. 4a, b).

To visualize NADPH and NADH dynamics *in vivo*, we microinjected mRNAs of iNap1 or SoNar into one-cell-stage zebrafish zygotes. Both sensors were expressed well, and their

fluorescence was visible in 2-d zebrafish larvae (Fig. 9a, b). H_2O_2 or the mitochondrial complex I inhibitor rotenone treatment induced a specific NADPH decrease and NADH increase, respectively, as shown by the fluorescence of the two sensors (Fig. 9a, b). To monitor NADPH and H_2O_2 dynamics *in vivo* simultaneously, we microinjected mRNAs of iNap1 and HyPerRed (H_2O_2 sensor) into a fertilized egg and observed a marked decrease in NADPH and increase in H_2O_2 levels at the wound margin in a previous study[8]. In zebrafish larvae simultaneously expressing SoNar and HyPerRed, H_2O_2 treatment induced a significant change in HyPerRed fluorescence, but not that of SoNar; conversely, rotenone treatment induced a significant change in SoNar fluorescence, but not that of HyPerRed (Fig. 9c, d). As a control, minimal changes in fluorescence were observed in iNapc-expressing zebrafish larvae with H_2O_2 or rotenone treatment (Supplementary Fig. 5a, b).

Supplementary Material

Refer to Web version on PubMed Central for supplementary material.

ACKNOWLEDGMENTS

We thank S.J. Remington for the roGFP1 vector; V.V. Belousov for the HyPer and HyPerRed vectors; Jiulin Du for the pTol2 vector; Jing Yi for the psPAX2 and pMD2.G vectors; Ni Su, Li Huang, Qiaohui Wang, Peili Ni and Huaxing Zi for technical assistance; and Stephanie C. Tribuna for secretarial assistance. This research is supported by National Key Research and Development Program of China (2017YFC0906900, 2017YFA050400, 2016YFA0100602, 2017YFA0103302), NSFC (31722033, 91649123, 31671484, 31225008, 31470833, 91749203, 81525010, 81420108017), the Shanghai Science and Technology Commission (14XD1401400, 16430723100, 15YF1402600), Young Elite Scientists Sponsorship Program by Cast, Shanghai Young Top-notch Talent, the State Key Laboratory of Bioreactor Engineering, the Fundamental Research Funds for the Central Universities, and US National Institutes of Health (HL061795, HG007690, and GM107618 to JL), and the American heart Association (D700382 to JL).

References:

1. Zhao Y, Zhang Z, Zou Y & Yang Y Visualization of Nicotine Adenine Dinucleotide Redox Homeostasis with Genetically Encoded Fluorescent Sensors. Antioxid Redox Signal 28, 213–229 (2018). [PubMed: 28648094]
2. Fan J et al. Quantitative flux analysis reveals folate-dependent NADPH production. Nature 510, 298–302 (2014). [PubMed: 24805240]
3. Cairns RA, Harris IS & Mak TW Regulation of cancer cell metabolism. Nat Rev Cancer 11, 85–95 (2011). [PubMed: 21258394]
4. Gorrini C, Harris IS & Mak TW Modulation of oxidative stress as an anticancer strategy. Nat Rev Drug Discov 12, 931–947 (2013). [PubMed: 24287781]
5. Ying W NAD+/NADH and NADP+/NADPH in cellular functions and cell death: regulation and biological consequences. Antioxid Redox Signal 10, 179–206 (2008). [PubMed: 18020963]
6. Blacker TS et al. Separating NADH and NADPH fluorescence in live cells and tissues using FLIM. Nat Commun 5, 3936 (2014). [PubMed: 24874098]
7. Maddocks OD, Labuschagne CF & Vousden KH Localization of NADPH production: a wheel within a wheel. Mol Cell 55, 158–160 (2014). [PubMed: 25038411]
8. Tao R et al. Genetically encoded fluorescent sensors reveal dynamic regulation of NADPH metabolism. Nat Methods 14, 720–728 (2017). [PubMed: 28581494]
9. Veech RL, Eggleston LV & Krebs HA The redox state of free nicotinamide-adenine dinucleotide phosphate in the cytoplasm of rat liver. Biochem J 115, 609–619 (1969). [PubMed: 4391039]
10. Canto C et al. AMPK regulates energy expenditure by modulating NAD+ metabolism and SIRT1 activity. Nature 458, 1056–1060 (2009). [PubMed: 19262508]

11. Wise DD & Shear JB Tracking variations in nicotinamide cofactors extracted from cultured cells using capillary electrophoresis with multiphoton excitation of fluorescence. Anal Biochem 326, 225–233 (2004). [PubMed: 15003563]
12. Lewis CA et al. Tracing compartmentalized NADPH metabolism in the cytosol and mitochondria of mammalian cells. Mol Cell 55, 253–263 (2014). [PubMed: 24882210]
13. Quinn KP et al. Quantitative metabolic imaging using endogenous fluorescence to detect stem cell differentiation. Sci Rep 3, 3432 (2013). [PubMed: 24305550]
14. Hanson GT et al. Investigating mitochondrial redox potential with redox-sensitive green fluorescent protein indicators. J Biol Chem 279, 13044–13053 (2004). [PubMed: 14722062]
15. Dooley CT et al. Imaging dynamic redox changes in mammalian cells with green fluorescent protein indicators. J Biol Chem 279, 22284–22293 (2004). [PubMed: 14985369]
16. Gutscher M et al. Real-time imaging of the intracellular glutathione redox potential. Nat Methods 5, 553–559 (2008). [PubMed: 18469822]
17. Fan Y, Chen Z & Ai HW Monitoring redox dynamics in living cells with a redox-sensitive red fluorescent protein. Anal Chem 87, 2802–2810 (2015). [PubMed: 25666702]
18. Belousov VV et al. Genetically encoded fluorescent indicator for intracellular hydrogen peroxide. Nat Methods 3, 281–286 (2006). [PubMed: 16554833]
19. Ermakova YG et al. Red fluorescent genetically encoded indicator for intracellular hydrogen peroxide. Nature communications 5, 5222 (2014).
20. Albrecht SC, Barata AG, Grosshans J, Teleman AA & Dick TP In vivo mapping of hydrogen peroxide and oxidized glutathione reveals chemical and regional specificity of redox homeostasis. Cell Metab 14, 819–829 (2011). [PubMed: 22100409]
21. Morgan B et al. Real-time monitoring of basal H2O2 levels with peroxiredoxin-based probes. Nat Chem Biol 12, 437–443 (2016). [PubMed: 27089028]
22. Zhao Y et al. SoNar, a highly responsive NAD+/NADH sensor, allows high-throughput metabolic screening of anti-tumor agents. Cell Metab 21, 777–789 (2015). [PubMed: 25955212]
23. Zhao Y et al. In vivo monitoring of cellular energy metabolism using SoNar, a highly responsive sensor for NAD(+)/NADH redox state. Nat Protoc 11, 1345–1359 (2016). [PubMed: 27362337]
24. Zhao Y et al. Genetically encoded fluorescent sensors for intracellular NADH detection. Cell Metab 14, 555–566 (2011). [PubMed: 21982715]
25. Wiederkehr A & Demaurex N Illuminating redox biology using NADH- and NADPH-specific sensors. Nat Methods 14, 671–672 (2017). [PubMed: 28661497]
26. Zhao Y & Yang Y Profiling metabolic states with genetically encoded fluorescent biosensors for NADH. Curr Opin Biotechnol 31C, 86–92 (2015).
27. Hung YP, Albeck JG, Tantama M & Yellen G Imaging Cytosolic NADH-NAD(+) Redox State with a Genetically Encoded Fluorescent Biosensor. Cell Metab 14, 545–554 (2011). [PubMed: 21982714]
28. Bilan DS et al. Genetically encoded fluorescent indicator for imaging NAD(+)/NADH ratio changes in different cellular compartments. Biochim Biophys Acta 1840, 951–957 (2014). [PubMed: 24286672]
29. Zhao Y & Yang Y Real-time and high-throughput analysis of mitochondrial metabolic states in living cells using genetically encoded NAD+/NADH sensors. Free Radic Biol Med 100, 43–52 (2016). [PubMed: 27261194]
30. Zhang J et al. Determination of the Cytosolic NADPH/NADP Ratio in Saccharomyces cerevisiae using Shikimate Dehydrogenase as Sensor Reaction. Sci Rep 5, 12846 (2015). [PubMed: 26243542]
31. Hedeskov CJ, Capito K & Thams P Cytosolic ratios of free [NADPH]/[NADP+] and [NADH]/[NAD+] in mouse pancreatic islets, and nutrient-induced insulin secretion. Biochem J 241, 161–167 (1987). [PubMed: 3551925]
32. Zhang Q, Piston DW & Goodman RH Regulation of corepressor function by nuclear NADH. Science 295, 1895–1897 (2002). [PubMed: 11847309]

33. Mayevsky A & Rogatsky GG Mitochondrial function in vivo evaluated by NADH fluorescence: from animal models to human studies. Am J Physiol Cell Physiol 292, C615–640 (2007). [PubMed: 16943239]
34. Murphy MP et al. Unraveling the biological roles of reactive oxygen species. Cell Metab 13, 361–366 (2011). [PubMed: 21459321]
35. Pollak N, Niere M & Ziegler M NAD kinase levels control the NADPH concentration in human cells. J Biol Chem 282, 33562–33571 (2007). [PubMed: 17855339]
36. Ohashi K, Kawai S & Murata K Identification and characterization of a human mitochondrial NAD kinase. Nat Commun 3, 1248 (2012). [PubMed: 23212377]
37. Cambronne XA et al. Biosensor reveals multiple sources for mitochondrial NAD(+). Science 352, 1474–1477 (2016). [PubMed: 27313049]
38. Cameron WD et al. Apollo-NADP(+): a spectrally tunable family of genetically encoded sensors for NADP(+). Nat Methods 13, 352–358 (2016). [PubMed: 26878383]
39. Hoek JB & Rydstrom J Physiological roles of nicotinamide nucleotide transhydrogenase. Biochem J 254, 1–10 (1988). [PubMed: 3052428]
40. Zhang X, Edwards JP & Mosser DM The expression of exogenous genes in macrophages: obstacles and opportunities. Methods Mol Biol 531, 123–143 (2009). [PubMed: 19347315]
41. Ghesquiere B, Wong BW, Kuchnio A & Carmeliet P Metabolism of stromal and immune cells in health and disease. Nature 511, 167–176 (2014). [PubMed: 25008522]
42. Karlsson J, von Hofsten J & Olsson PE Generating transparent zebrafish: a refined method to improve detection of gene expression during embryonic development. Mar Biotechnol (NY) 3, 522–527 (2001). [PubMed: 14961324]
43. Fan Y & Ai HW Development of redox-sensitive red fluorescent proteins for imaging redox dynamics in cellular compartments. Anal Bioanal Chem 408, 2901–2911 (2016). [PubMed: 26758595]
44. Villalobos A, Ness JE, Gustafsson C, Minshull J & Govindarajan S Gene Designer: a synthetic biology tool for constructing artificial DNA segments. BMC Bioinformatics 7, 285 (2006). [PubMed: 16756672]
45. Schwartz MA, Schaller MD & Ginsberg MH Integrins: emerging paradigms of signal transduction. Annual review of cell and developmental biology 11, 549–599 (1995).
46. Hynes RO Integrins: versatility, modulation, and signaling in cell adhesion. Cell 69, 11–25 (1992). [PubMed: 1555235]
47. Tiscornia G, Singer O & Verma IM Production and purification of lentiviral vectors. Nat Protoc 1, 241–245 (2006). [PubMed: 17406239]
48. Q. X Microinjection into Zebrafish Embryos, In: Guille M (eds) Molecular Methods in Developmental Biology. Methods Mol Biol 127, 125–132 (1999).
49. Kelsh RN et al. Zebrafish pigmentation mutations and the processes of neural crest development. Development 123, 369–389 (1996). [PubMed: 9007256]
50. Inaba M, Yamanaka H & Kondo S Pigment pattern formation by contact-dependent depolarization. Science 335, 677 (2012). [PubMed: 22323812]
51. Ma X et al. Polo-like kinase 1 coordinates biosynthesis during cell cycle progression by directly activating pentose phosphate pathway. Nat Commun 8, 1506 (2017). [PubMed: 29138396]
52. Noda T & Amano F Differences in nitric oxide synthase activity in a macrophage-like cell line, RAW264.7 cells, treated with lipopolysaccharide (LPS) in the presence or absence of interferon-gamma (IFN-gamma): possible heterogeneity of iNOS activity. J Biochem 121, 38–46 (1997). [PubMed: 9058189]
53. Lohman JR & Remington SJ Development of a family of redox-sensitive green fluorescent protein indicators for use in relatively oxidizing subcellular environments. Biochemistry 47, 8678–8688 (2008). [PubMed: 18652491]
54. Ostergaard H, Henriksen A, Hansen FG & Winther JR Shedding light on disulfide bond formation: engineering a redox switch in green fluorescent protein. EMBO J 20, 5853–5862 (2001). [PubMed: 11689426]

55. Markvicheva KN et al. A genetically encoded sensor for H2O2 with expanded dynamic range. Bioorg Med Chem 19, 1079–1084 (2011). [PubMed: 20692175]

56. Bilan DS et al. HyPer-3: a genetically encoded H2O2 probe with improved performance for ratiometric and fluorescence lifetime imaging. ACS Chem Biol 8, 535–542 (2013). [PubMed: 23256573]

57. Williamson DH, Lund P & Krebs HA The redox state of free nicotinamide-adenine dinucleotide in the cytoplasm and mitochondria of rat liver. Biochem J 103, 514–527 (1967). [PubMed: 4291787]

EDITORIAL SUMMARY

This protocol describes how to combine up to four genetically encoded fluorescent sensors to image redox landscapes and dynamics. The Procedures describe applications in live imaging flow cytometry of cultured cells, and in vivo imaging in zebrafish larvae.

TWEET

A new protocol describing how to combine up to four genetically encoded fluorescent sensors to image redox landscapes and dynamics in cells and in zebrafish larvae.

COVER TEASER

Combined imaging of multiple redox sensors

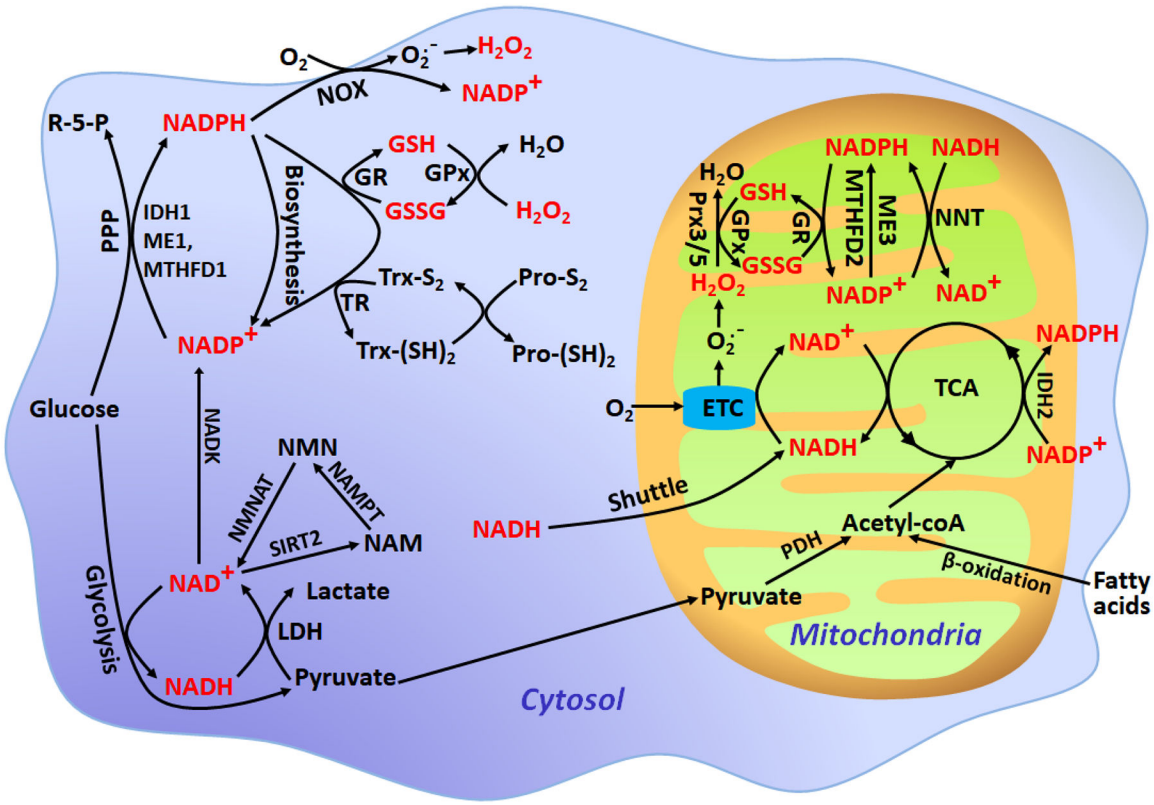

Figure 1. Simplified schematic of intracellular redox buffering systems.

R-5-P, ribulose 5-phosphate; ME1/3, malic enzyme 1/3; IDH1/2, isocitrate dehydrogenase 1/2; MTHFD1/2, methylene tetrahydrofolate dehydrogenase 1/2; NNT, nicotinamide nucleotide transhydrogenase; SIRT2, sirtuin 2; NAMPT, nicotinamide phosphoribosyltransferase; NMNAT, nicotinamide mononucleotide adenylyltransferase; LDH, lactate dehydrogenase; PDH, pyruvate dehydrogenase; GR, glutathione reductase; TR, thioredoxin reductase; GSSG, oxidized glutathione; GSH, reduced glutathione; Trx-S_2, oxidized thioredoxin; Trx-$(SH)_2$, reduced thioredoxin; GPx, glutathione peroxidase; Prx3/5, peroxiredoxin 3/5; Pro-S_2, proteins with disulfide bonds; Pro-$(SH)_2$, proteins with reduced thiols; NOX, NADPH oxidase.

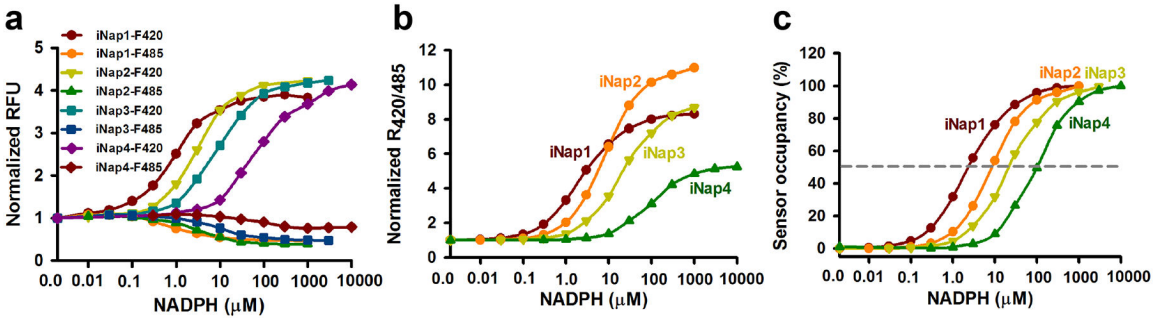

Figure 2. Properties of iNap1–4 sensors.

(**a**) iNap1-iNap4 fluorescence intensity at an excitation of 420 nm (F420) or 485 nm (F485) in the presence of different concentrations of NADPH. Emission was measured at 528 nm. (**b**) Normalized NADPH titration curves of iNap1-iNap4 sensors. (**c**) Occupancy of iNap1-iNap4 sensors. Binding affinities for NADPH were determined as 2 μM, 6 μM, 25 μM and 120 μM, respectively.

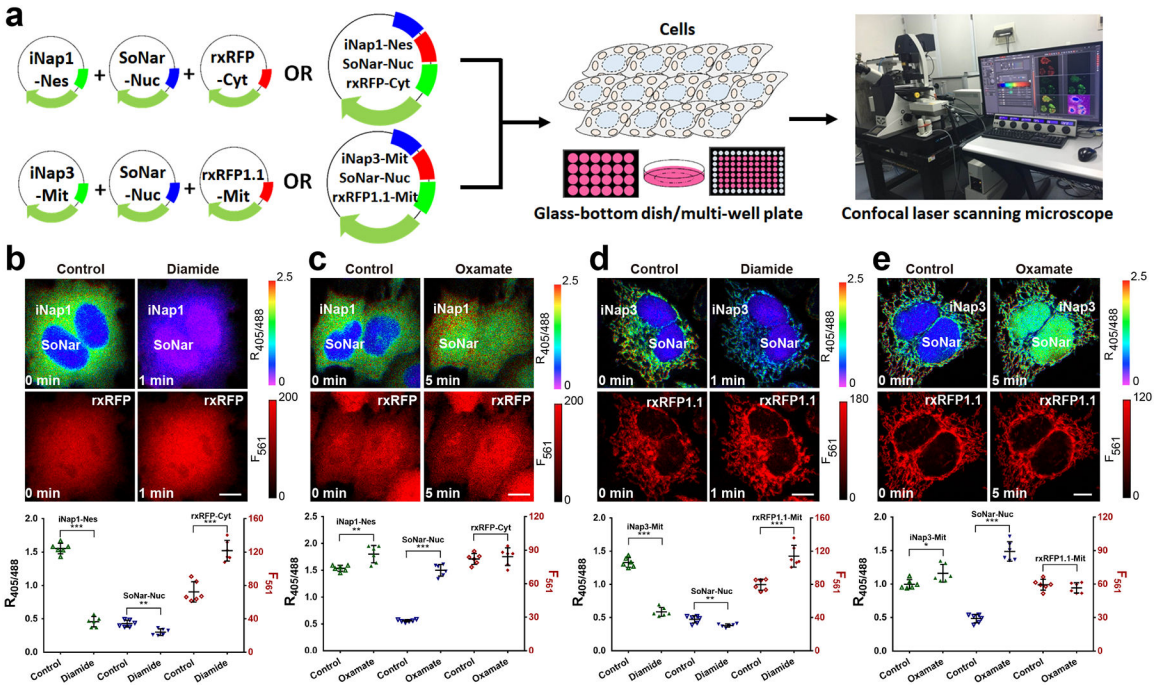

Figure 3. Three-parametric imaging of NADPH, NADH, and thiol redox state in single cells.

(**a**) General overview of the procedure for three-parametric imaging in single cells. (**b** and **c**) Three-parametric imaging (top) and fluorescence changes (bottom, n=6 cells) in HeLa cells simultaneously expressing nuclear-excluded iNap1, nuclear-localized SoNar, and cytosol-localized rxRFP in response to 200 μM diamide (b) or 2 mM oxamate (c). (**d** and **e**) Three-parametric imaging (top) and fluorescence changes (bottom, n=6 cells) in HeLa cells simultaneously expressing mitochondrial-localized iNap3, nuclear-localized SoNar, and mitochondrial-localized rxRFP1.1 in response to 200 μM diamide (d) or 2 mM oxamate (e). Data are the mean ± s.d. All *p* values were obtained using unpaired two-tailed Student's t test. $*p < 0.05$,$**p < 0.01$, $***p < 0.001$. Scale bars, 10 μm.

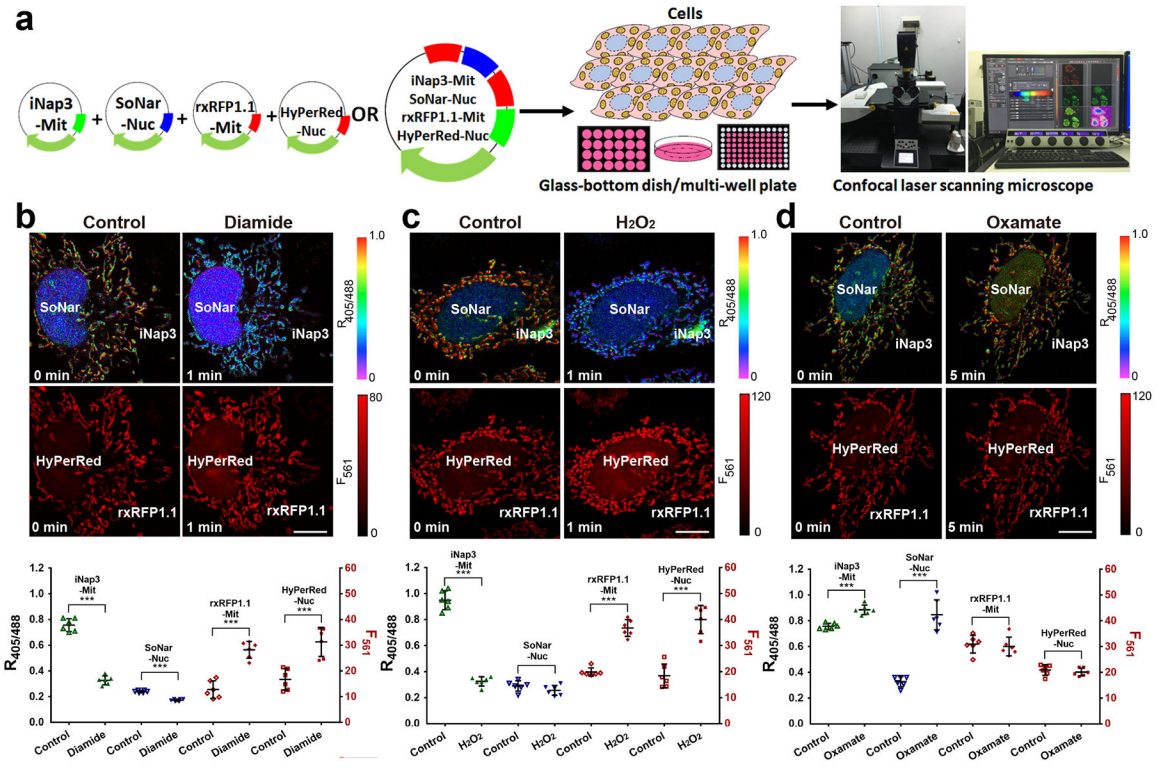

Figure 4. Four-parametric imaging of NADPH, NADH, thiol redox, and H_2O_2 in single cells.

(**a**) General overview of the procedure for four-parametric imaging in single cells. (**b-d**) Four-parametric imaging (top) and fluorescence changes (bottom, n=6 cells) in HeLa cells simultaneously expressing mitochondrial-localized iNap3, nuclear-localized SoNar, mitochondrial-localized rxRFP1.1, and nuclear-localized HyPerRed in response to 200 μM diamide (b), 200 μM H_2O_2 (c), or 2 mM oxamate (d). Data are the mean ± s.d. All *p* values were obtained using unpaired two-tailed Student's t test. ***$p < 0.001$. Scale bars, 10 μm.

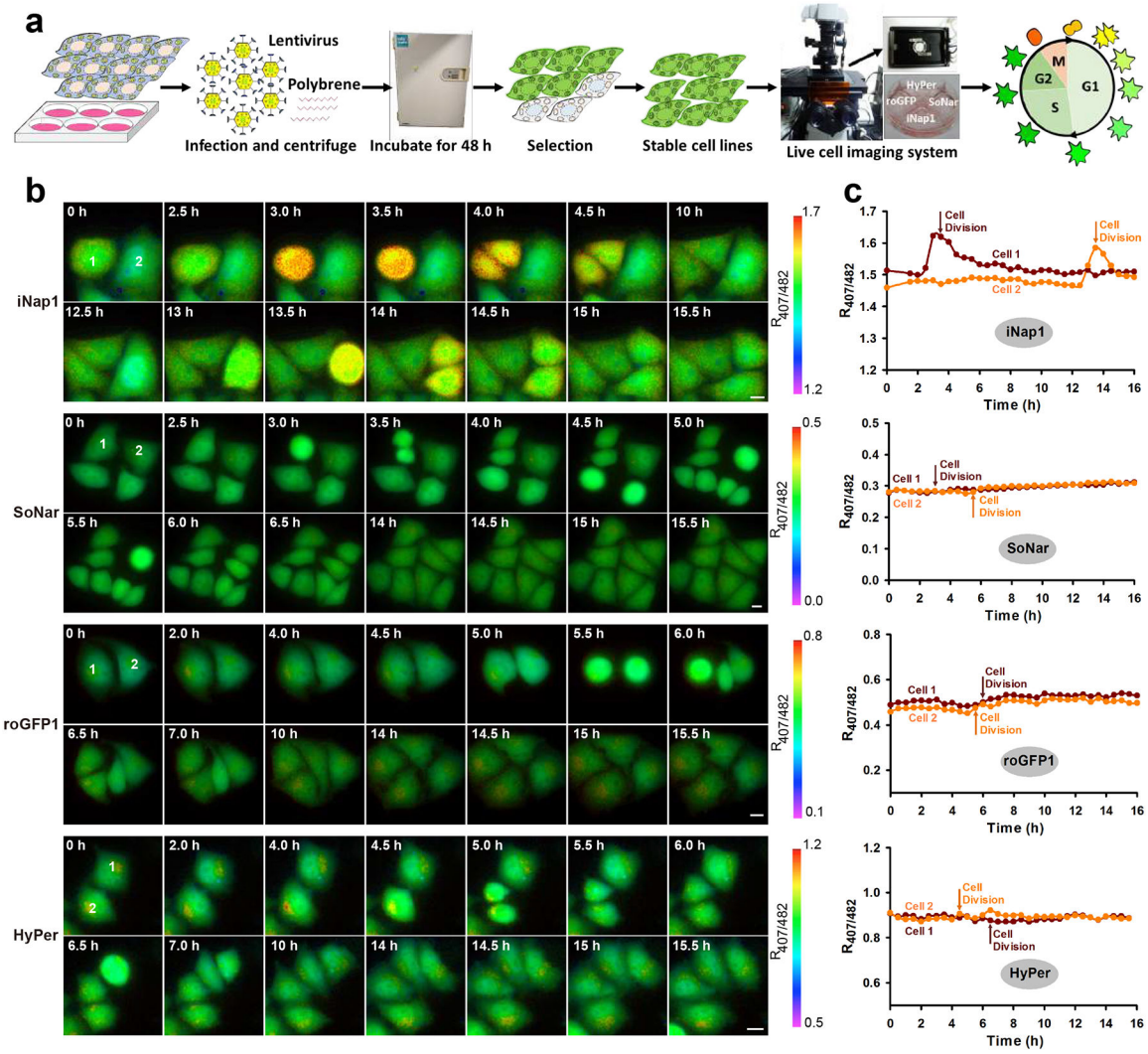

Figure 5. Real-time monitoring of NADPH, NADH, thiol redox, and H_2O_2 dynamics during the cell cycle.

(**a**) General overview of the procedure for multiple imaging of redox landscapes and dynamics during the cell cycle. (**b** and **c**) Fluorescence images (b) and quantification (c) of NADPH, NADH, thiol redox, and H_2O_2 dynamics during cell division. Scale bars, 10 μm.

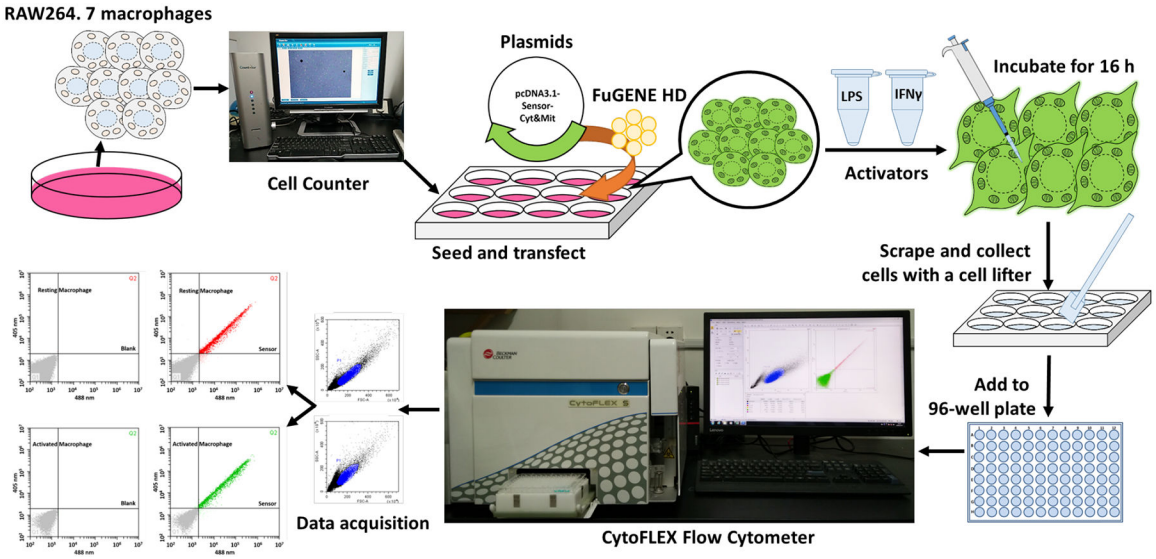

Figure 6. Overview of flow cytometry analysis.

General overview of the procedure for redox sensor-based flow cytometry analysis during macrophage activation.

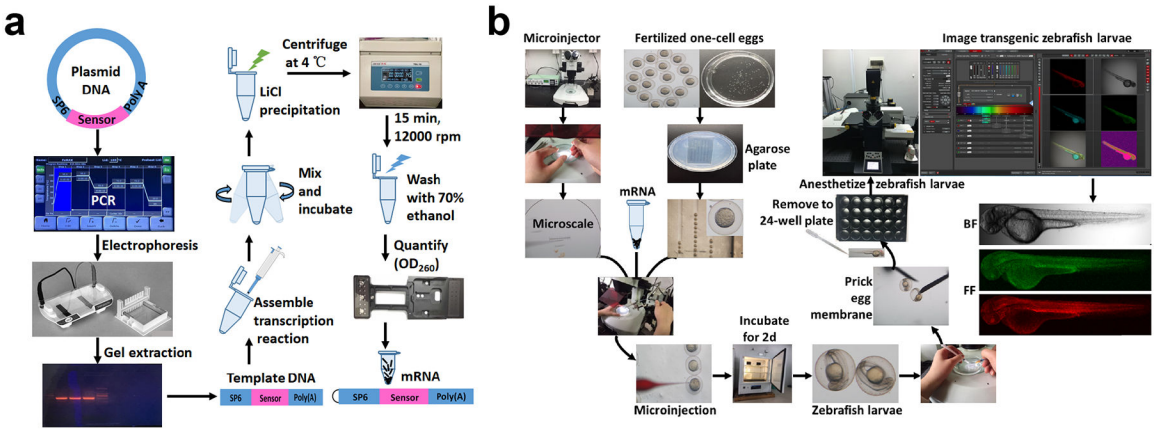

Figure 7. Overview of zebrafish imaging.

All procedures involving animals were approved by the Institutional Animal Care and Use Committee of Shanghai Institutes for Biological Sciences. (**a** and **b**) General procedures of sensor mRNA preparation (a) and zebrafish imaging (b).

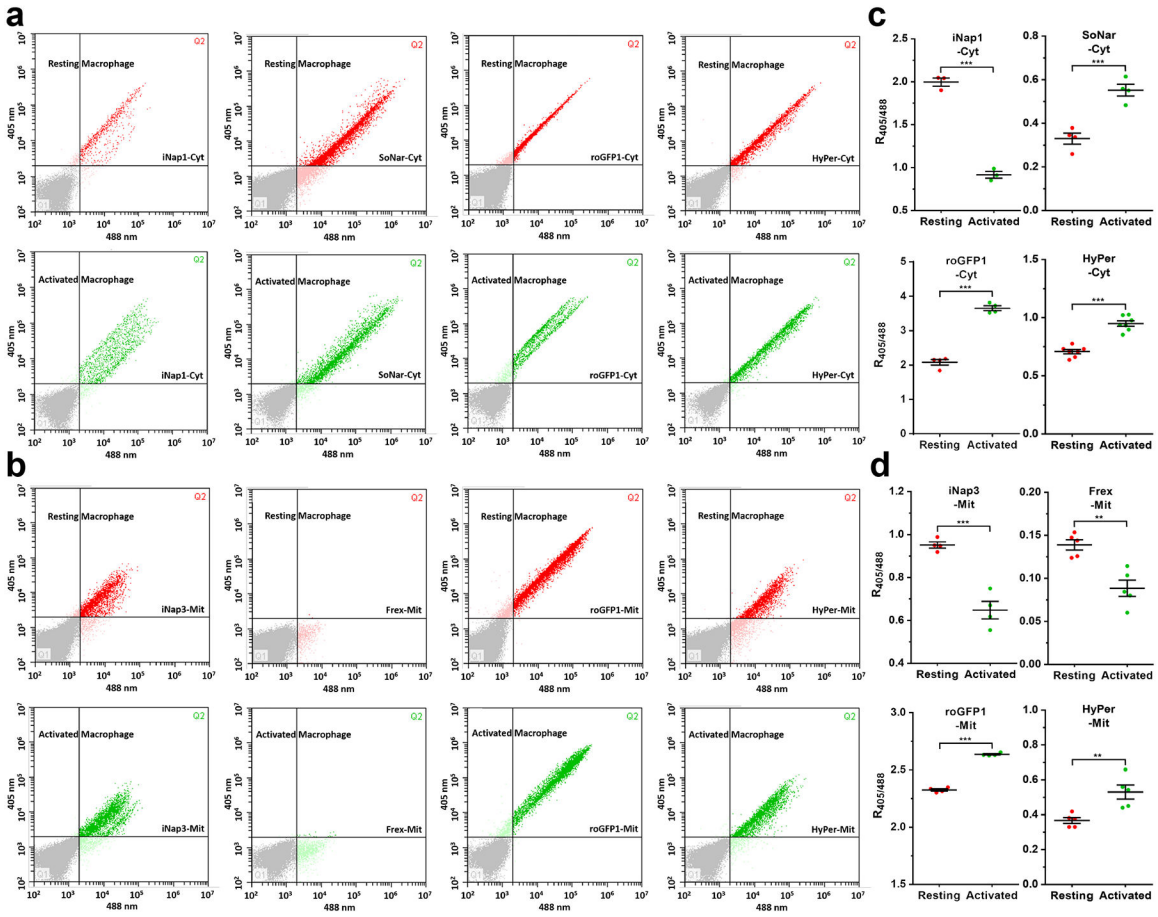

Figure 8. Comprehensive analysis of cytosolic and mitochondrial redox state in resting and activated mouse macrophages by flow cytometry.

(**a** and **b**) Cytosolic (a) or mitochondrial (b) NADPH, NADH, thiol redox, and H_2O_2 detection in resting or activated RAW264.7 mouse macrophages by flow cytometry. (**c** and **d**) Quantitative data for cytosolic (c) or mitochondrial (d) sensor fluorescence were obtained from three or more independent assessments by flow cytometry. Data are the mean ± s.e.m. All *p* values were obtained using unpaired two-tailed Student's t test. $^{**}p < 0.01$, $^{***}p < 0.001$.

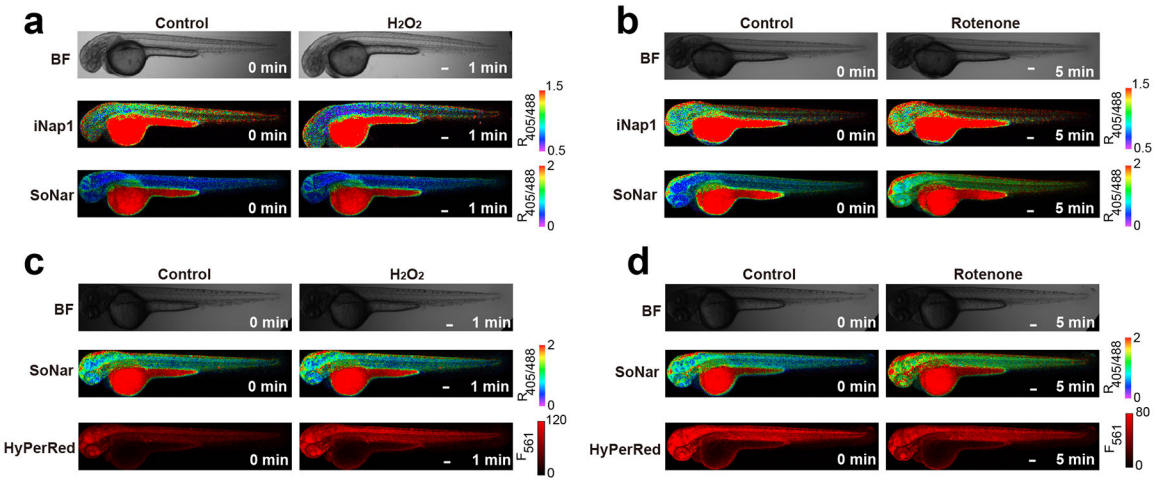

Figure 9. Spatiotemporal imaging of NADPH, NADH, and H_2O_2 in living zebrafish.

All procedures involving animals were approved by the Institutional Animal Care and Use Committee of Shanghai Institutes for Biological Sciences. (**a** and **b**) *In vivo* fluorescence imaging of zebrafish larvae expressing iNap1 or SoNar in response to 50 mM H_2O_2 (a) or 5 μM rotenone (b). BF = bright field. (**c** and **d**) Simultaneous visualization of NADH and H_2O_2 dynamics in response to 50 mM H_2O_2 (c) or 5 μM rotenone (d) by coexpression of SoNar and HyPerRed in zebrafish larvae. Scale bars, 100 μm.

Table 1 |

Properties of genetically encoded redox sensors.

	Sensor	Species sensed	Dynamic changes(%)	K_d or Midpoint Potential	Fluorescent protein	Detection mode	Sensor type	pH sensitivity
NADPH/NADP$^+$	iNap1[8]	NADPH	900	~2 μM;	cpYFP	Fluorescence intensity	Ratiometric	Resistant[a]
	iNap2[8]		1000	~6.4 μM;				
	iNap3[8]		900	~25 μM;				
	iNap4[8]		500	~120 μM;				
	Apollo-NADP$^+$[38]	NADP$^+$	15–20	0.1–20 μM	FP	Fluorescence anisotropy	Ratiometric	Resistant
NADH/NAD$^+$	Frex[24]	NADH	800	~3.7 μM; ~11 μM[b]	cpYFP	Fluorescence intensity	Ratiometric	Sensitive
	LigA-cpVenus[37]	NAD$^+$	100	~65 μM	cpVenus	Fluorescence intensity	Ratiometric	Sensitive
	SoNar[22,23]	NADH/NAD$^+$ ratio	1500	~40	cpYFP	Fluorescence intensity	Ratiometric	Resistant[a]
	Peredox[27]	NADH/NAD$^+$ ratio	150	~330	cpT-Sapphire	Fluorescence intensity	Intensiometric	Resistant
	RexYFP[28]	NADH/NAD$^+$ ratio	50	N.D.	cpYFP	Fluorescence intensity	Intensiometric	Sensitive
-SH/-SS-	roGFP1[14,15]	-SH/-SS-	350	−288 mV	GFP	Fluorescence intensity	Ratiometric	Resistant
	roGFP2[14,15]		480	−272mV				Sensitive
	roGFP-iX[53]		140–620	−229 to −246 mV				Sensitive
	rxRFP[17,43]	-SH/-SS-	400	−290 mV	cpmApple	Fluorescence intensity	Intensiometric	Sensitive
	rxYFP[54]	-SH/-SS-	300	−261 mV	YFP	Fluorescence intensity	Intensiometric	Sensitive
	Grx1-roGFP2[16]	GSSG/GSH	800	−280 mV	roGFP2	Fluorescence intensity	Ratiometric	Resistant
H_2O_2	HyPer[18]	H_2O_2	200	−185 mV	cpYFP	Fluorescence intensity	Ratiometric	Sensitive
	HyPer2[55]		500	N.D.				
	HyPer3[56]		450	N.D.				
	HyPerRed[19]	H_2O_2	80	N.D.	cpmApple	Fluorescence intensity	Intensiometric	Sensitive
	roGFP2-Orp1[20]	H_2O_2	410–510	N.D.	roGFP2	Fluorescence intensity	Ratiometric	Resistant
	roGFP2-Tsa2ΔC$_R$[21]	H_2O_2	500	N.D.	roGFP2	Fluorescence intensity	Ratiometric	Resistant

N.D., not determined. FP, Fluorescent protein

[a] iNap's or SoNar's fluorescence excited at 420 nm, dynamic range, and K_d are pH resistant.

[b] The apparent NADH dissociation constant (K_d) of Frex was ~3.7 μM at pH 7.4 and ~11 μM at pH 8.0, respectively.

Table 2 |

Cytosolic and mitochondrial-free NADPH, $NADP^+$, NADPH/$NADP^+$ ratio, NADH, NAD^+, and NADH/NAD^+ ratio in mammalian cells.

	Cytosol	Mitochondria	reference
NADPH	~3.1 μM	~37 μM	8
$NADP^+$	~9.3–200 nM	~185 nM	*a*
NADPH/$NADP^+$ ratio	15–333	200	9,31,39
NADH	~0.12 μM	~30 μM	24
NAD^+	~106 μM	~230 μM	37
NADH/NAD^+ ratio	0.001–0.0167	0.1–0.25	23,57

*a*Cytosolic and mitochondrial-free $NADP^+$ was calculated from the free NADPH level[8] and free $NADP^+$/NADPH ratio[9,31,39] in mammalian cells.

Table 3

Overview of plasmids used in this study.

Name	Target	Excitation (nm)	Emission (nm)	Targeting	Cell type	Source
pRSETB-iNap1–4	NADPH	420/500	515	Cytosol	E. coli	Ref.[8]
pcDNA3.1/Hygro$^{(+)}$-cyt-iNap1	NADPH	420/500	515	Cytosol	Mammalian	Ref.[8]
pcDNA3.1/Hygro$^{(+)}$-nes-iNap1	NADPH	420/500	515	Nucleus-excluded	Mammalian	Ref.[8]
pLVX-cyt-iNap1	NADPH	420/500	515	Cytosol	Mammalian	Ref.[8]
pTol2-iNap1	NADPH	420/500	515	Cytosol	Zebrafish	Ref.[8]
pcDNA3.1/Hygro$^{(+)}$-mit-iNap3	NADPH	420/500	515	Mitochondria	Mammalian	Ref.[8]
pcDNA3.1/Hygro$^{(+)}$-cyt-iNapc	pH	420/500	515	Cytosol	Mammalian	Ref.[8]
pcDNA3.1/Hygro$^{(+)}$-nuc-iNapc	pH	420/500	515	Nucleus	Mammalian	Ref.[8]
pcDNA3.1/Hygro$^{(+)}$-mit-iNapc	pH	420/500	515	Mitochondria	Mammalian	Ref.[8]
pLVX-cyt-iNapc	pH	420/500	515	Cytosol	Mammalian	Ref.[8]
pTol2-iNapc	pH	420/500	515	Cytosol	Zebrafish	Ref.[8]
pcDNA3.1/Hygro$^{(+)}$-cyt-SoNar	NADH/NAD$^+$ ratio	420/500	518	Cytosol	Mammalian	Ref.[22]
pcDNA3.1/Hygro$^{(+)}$-nuc-SoNar	NADH/NAD$^+$ ratio	420/500	518	Nucleus	Mammalian	Ref.[22]
pLVX-cyt-SoNar	NADH/NAD$^+$ ratio	420/500	518	Cytosol	Mammalian	Ref.[22]
pTol2-SoNar	NADH/NAD$^+$ ratio	420/500	518	Cytosol	Zebrafish	Ref.[22]
pcDNA3.1/Hygro$^{(+)}$-mit-Frex	NADH	420/500	518	Mitochondria	Mammalian	Ref.[24]
pcDNA3.1/Hygro$^{(+)}$-cyt-cpYFP	pH	420/500	518	Cytosol	Mammalian	Ref.[24]
pcDNA3.1/Hygro$^{(+)}$-mit-cpYFP	pH	420/500	518	Mitochondria	Mammalian	Ref.[24]
pcDNA3.1/Hygro$^{(+)}$-cyt-rxRFP[a]	-SH/-SS-	576	600	Cytosol	Mammalian	Ref.[17]
pcDNA3.1/Hygro$^{(+)}$-mit-rxRFP1.1[a]	-SH/-SS-	576	600	Mitochondria	Mammalian	Ref.[43]
pcDNA3.1/Hygro$^{(+)}$-cyt-pHRFP[a]	pH	576	600	Cytosol	Mammalian	Ref.[17]
pcDNA3.1/Hygro$^{(+)}$-mit-pHRFP[a]	pH	576	600	Mitochondria	Mammalian	Ref.[17]
pEGFP-N1-cyt-roGFP1	-SH/-SS-	400/490	515	Cytosol	Mammalian	Ref.[10,11]
pEGFP-N1-mit-roGFP1	-SH/-SS-	400/490	515	Mitochondria	Mammalian	Ref.[10,11]
pLVX-cyt-roGFP1	-SH/-SS-	400/490	515	Cytosol	Mammalian	Ref.[10,11]
pcDNA3.1/Hygro$^{(+)}$-cyt-HyPer	H_2O_2	420/500	516	Cytosol	Mammalian	Ref.[18]
pcDNA3.1/Hygro$^{(+)}$-mit-HyPer	H_2O_2	420/500	516	Mitochondria	Mammalian	Ref.[18]
pLVX-cyt-HyPer	H_2O_2	420/500	516	Cytosol	Mammalian	Ref.[18]
pcDNA3.1/Hygro$^{(+)}$-nuc-HyPerRed	H_2O_2	575	605	Nucleus	Mammalian	Ref.[19]

Name	Target	Excitation (nm)	Emission (nm)	Targeting	Cell type	Source
pTol2-HyPerRed	H_2O_2	575	605	Cytosol	Zebrafish	Ref.[19]

Δ CRITICAL All plasmids are available upon request.

[a]The rxRFP, rxRFP1.1 and pHRFP sensors are synthesized according to the cDNA sequences reported by Hui-wang Ai[43] (Addgene plasmid #67830, Addgene plasmid #67841, and Addgene plasmid #67832, respectively).

Table 4 |

Troubleshooting Table

Step	Problem	Possible reason	Solution
1	Failure of protein expression	The OD_{600} value is too high	Adjust the OD_{600} value
		Host strains are not appropriate	Choose appropriate expression strains such as BL21(DE3), BL21(DE3) pLysS, JM109(DE3)
5	Poor cell attachment	Glass-bottom surface is not ideal for cell attachment	Coat the glass-bottom plate or dish with poly-D-lysine, fibronectin or collagen, etc.
9	The number of cells simultaneously expressing multiple sensors is scarce	The proportion of sensor plasmids is not appropriate	Increase the proportion of low-expression sensor
		Low transfection efficiency or cell death	Optimize the transfection conditions
9	Blurry images	Image out of focus	Pipette carefully
		Adaptive focus control (AFC) has been shut down	Open AFC before imaging
		Super-sensitive HyD hybrid detector is close	Open HyD detector before imaging
9	Overexposure of the image during cell cycle	Fluorescence intensity significantly increases during the M phase of the cell cycle	Shorten the exposure time Lower the light intensity Lower the gain
12	Low transfection efficiency of RAW264.7 cells	Misuse of liposomal transfection reagents	Use of nonliposomal transfection reagent (i.e., FuGENE HD)
31	Zebrafish only expresses one sensor for multi-color image	The injection dose of mRNA for the low-expression sensor is low mRNA degradation of the low-expression sensor	Increase the proportion of low-expression sensor and the total mRNA Store in small aliquots at −80°C and avoid repeated refreezing and thawing of mRNA
31	Most zebrafish are dead or lack fluorescence	The viability of fertilized eggs is low	Choose high-viability eggs
		The quality of mRNA is poor	Choose high-quality mRNA
		The injection dose of mRNA is too high	Reduce the dosage of mRNA
31	Zebrafish twist or move during imaging	Inadequate anesthesia	Sufficiently anesthetize zebrafish larvae by adjusting the dose of tricaine; 1% low-melting agarose can be used to mount the larvae and minimize movement